Supporting Information

For

Indium Alkoxide Complexes Supported by Constrained Schiff-base Ligands for the Ring-opening (Co)polymerization of Cyclic Esters

Thitirat Piyawongsiri, Phongnarin Chumsaeng, and Khamphee Phomphrai*

Department of Materials Science and Engineering,
School of Molecular Science and Engineering,
Vidyasirimedhi Institute of Science and Technology (VISTEC)
Wangchan, Rayong 21210, Thailand
E-mail: khamphee.p@vistec.ac.th

Table of Contents

Comparison of O–OH Distances in 5-, 6-, and 7-Membered Rings

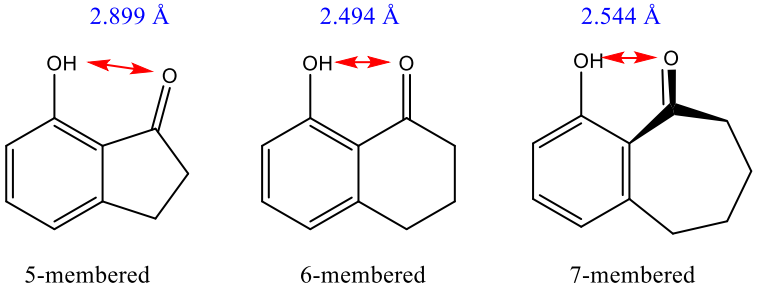

Figure S1. Comparison of Keto-Phenoxy O–OH Distances in 5-, 6-, and 7-Membered Rings

NMR Spectra of complex 2a-c

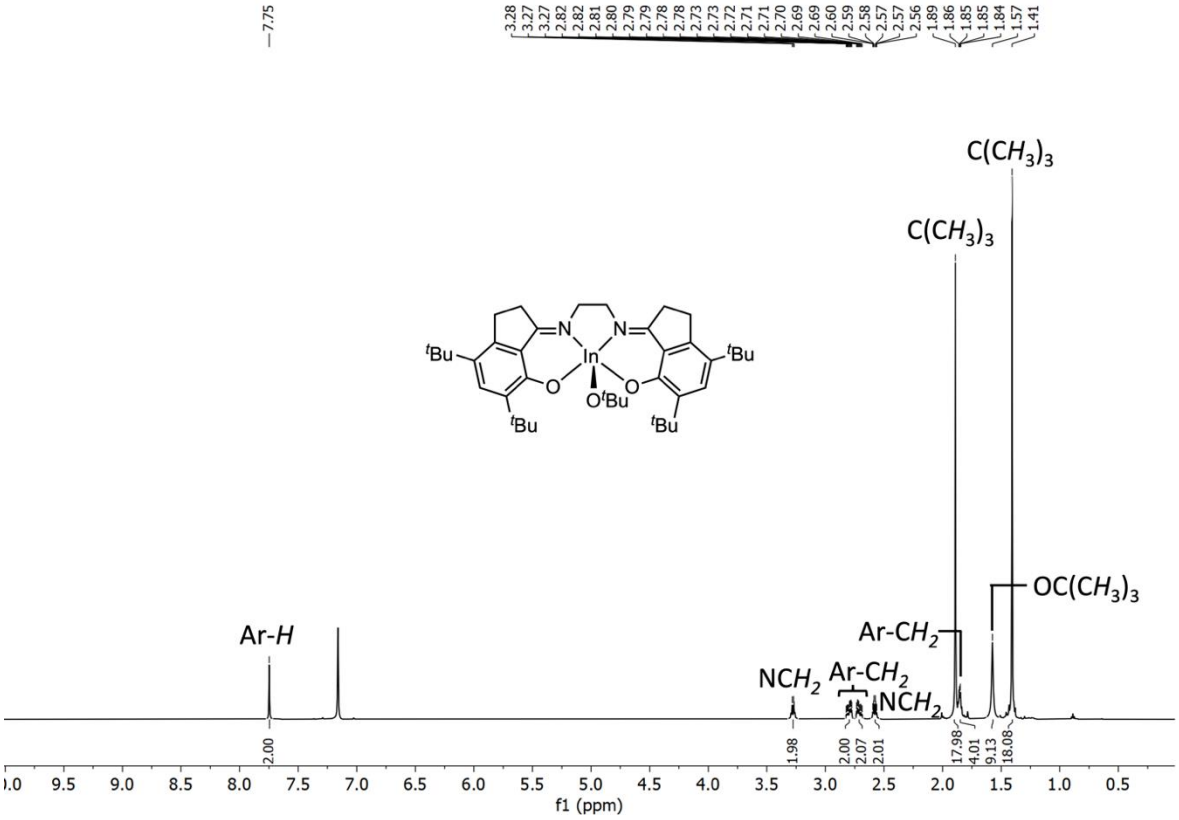

Figure S2. ^{1}H NMR spectrum (600 MHz, C_6D_6, 30 °C) of complex **2a.**

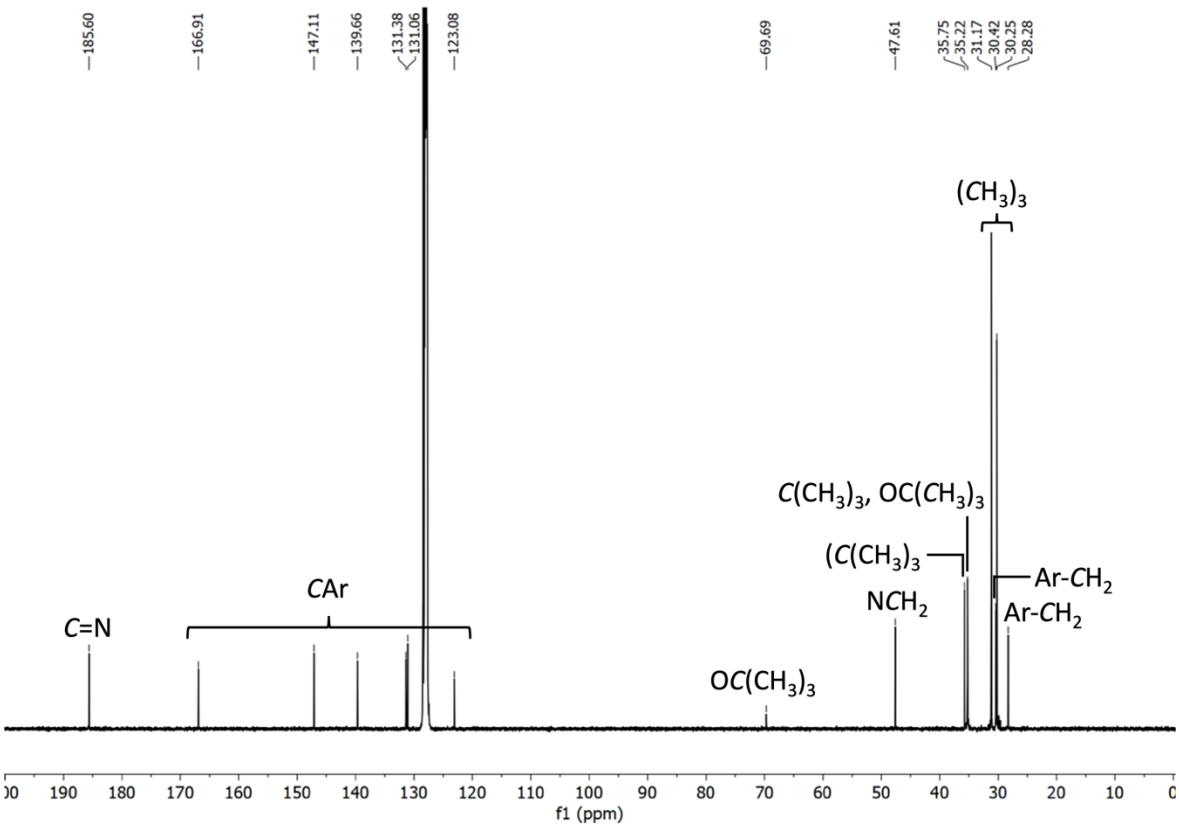

Figure S3. ^{13}C NMR spectrum (150 MHz, C_6D_6, 30 °C) of complex **2a.**

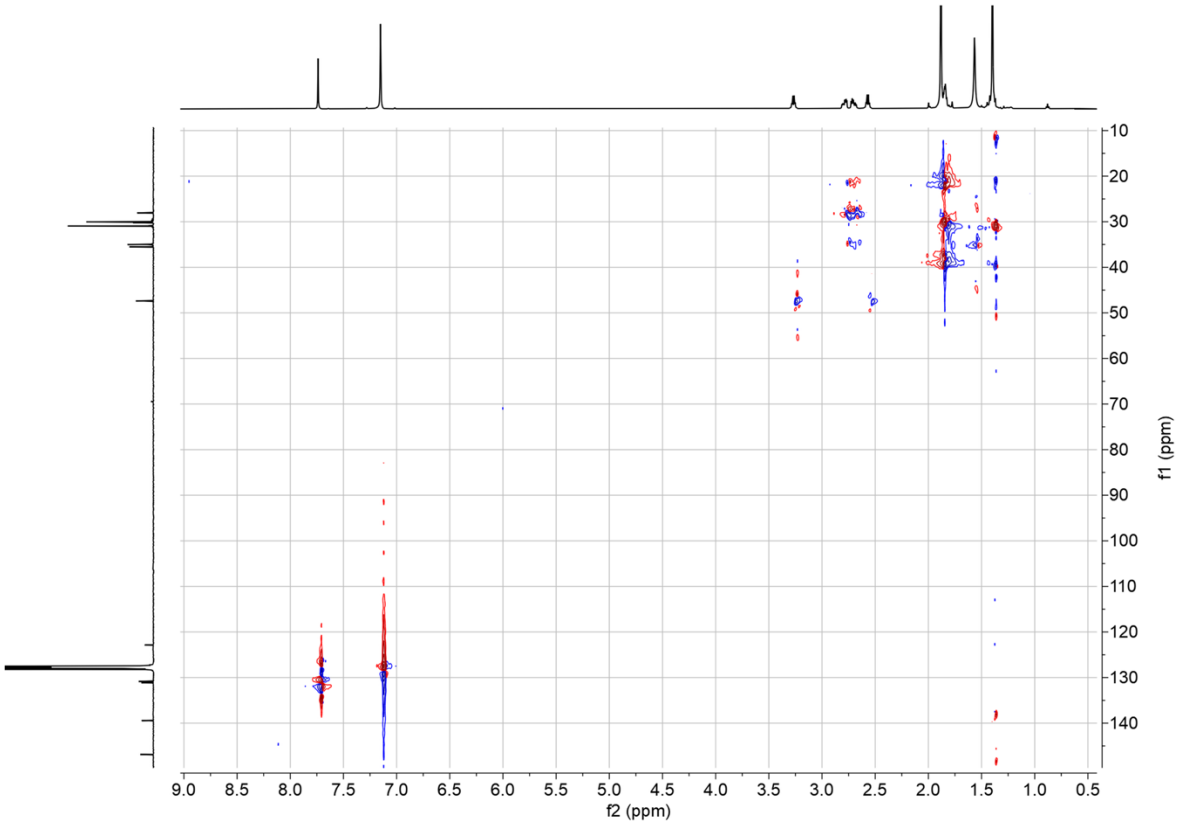

Figure S4. HSQC NMR spectrum (600 MHz, C_6D_6, 30 °C) of complex **2a.**

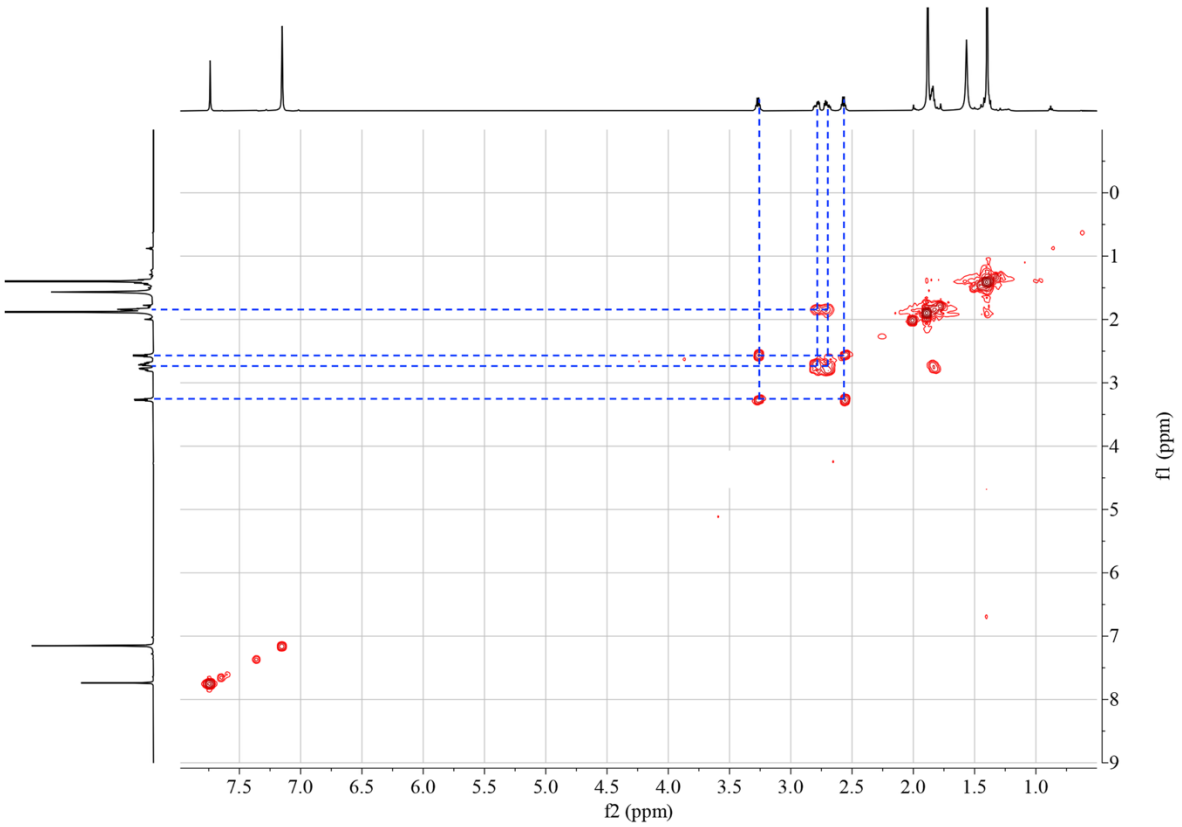

Figure S5. COSY NMR spectrum (600 MHz, C_6D_6, 30 °C) of complex **2a.**

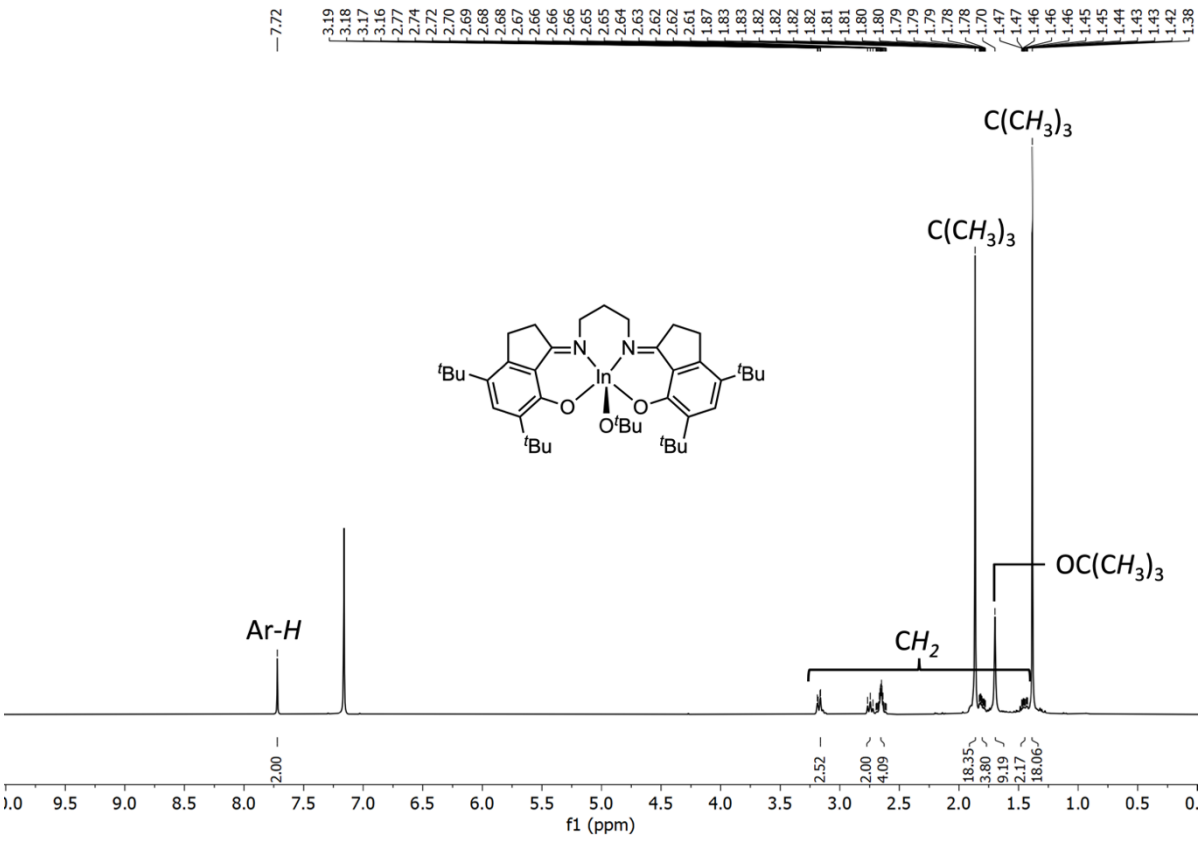

Figure S6. ^{1}H NMR spectrum (600 MHz, C_6D_6, 30 °C) of complex **2b.**

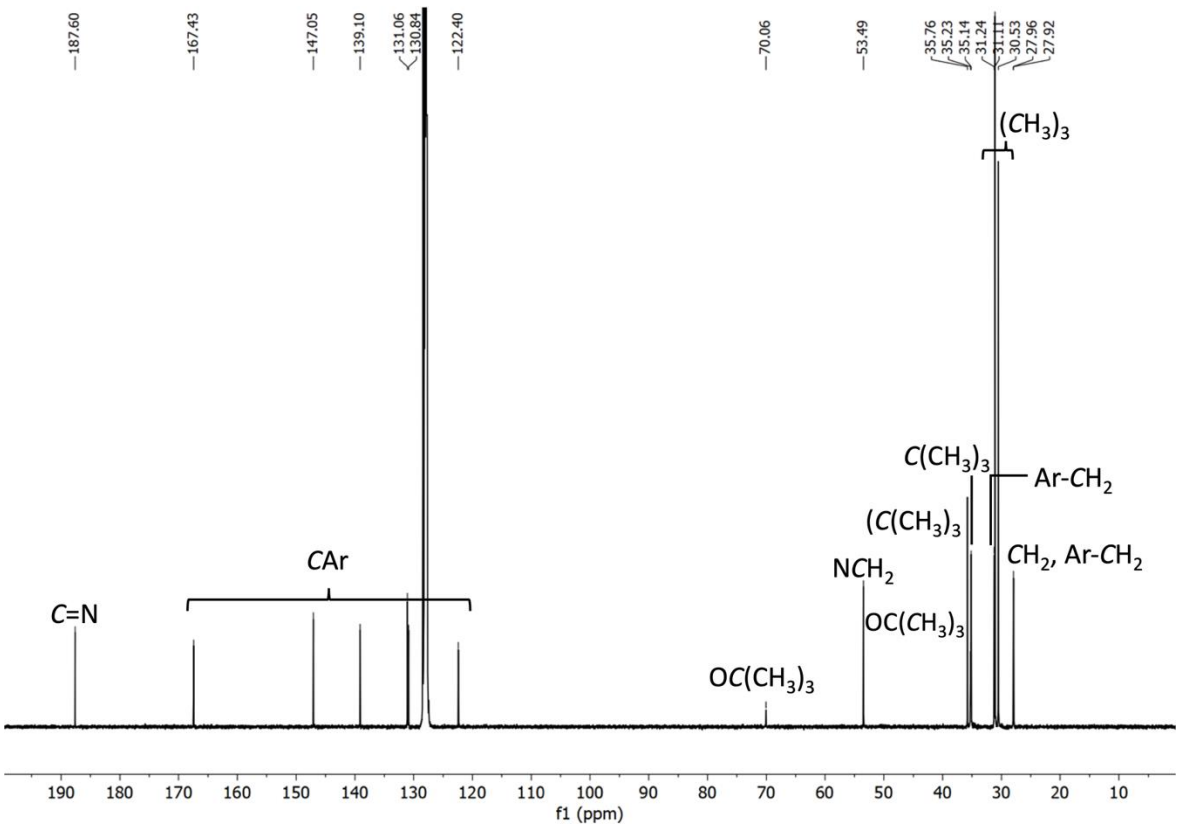

Figure S7. ^{13}C NMR spectrum (150 MHz, C_6D_6, 30 °C) of complex **2b.**

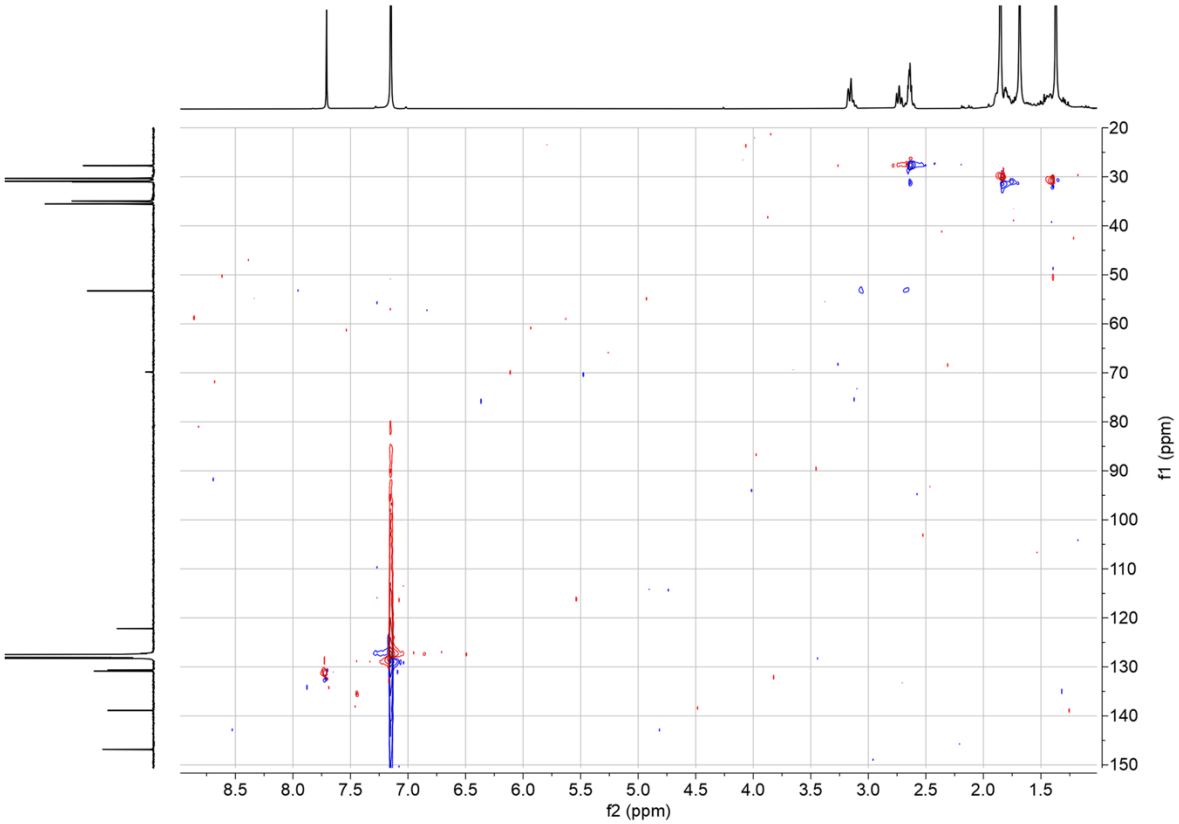

Figure S8. HSQC NMR spectrum (600 MHz, C_6D_6, 30 °C) of complex **2b.**

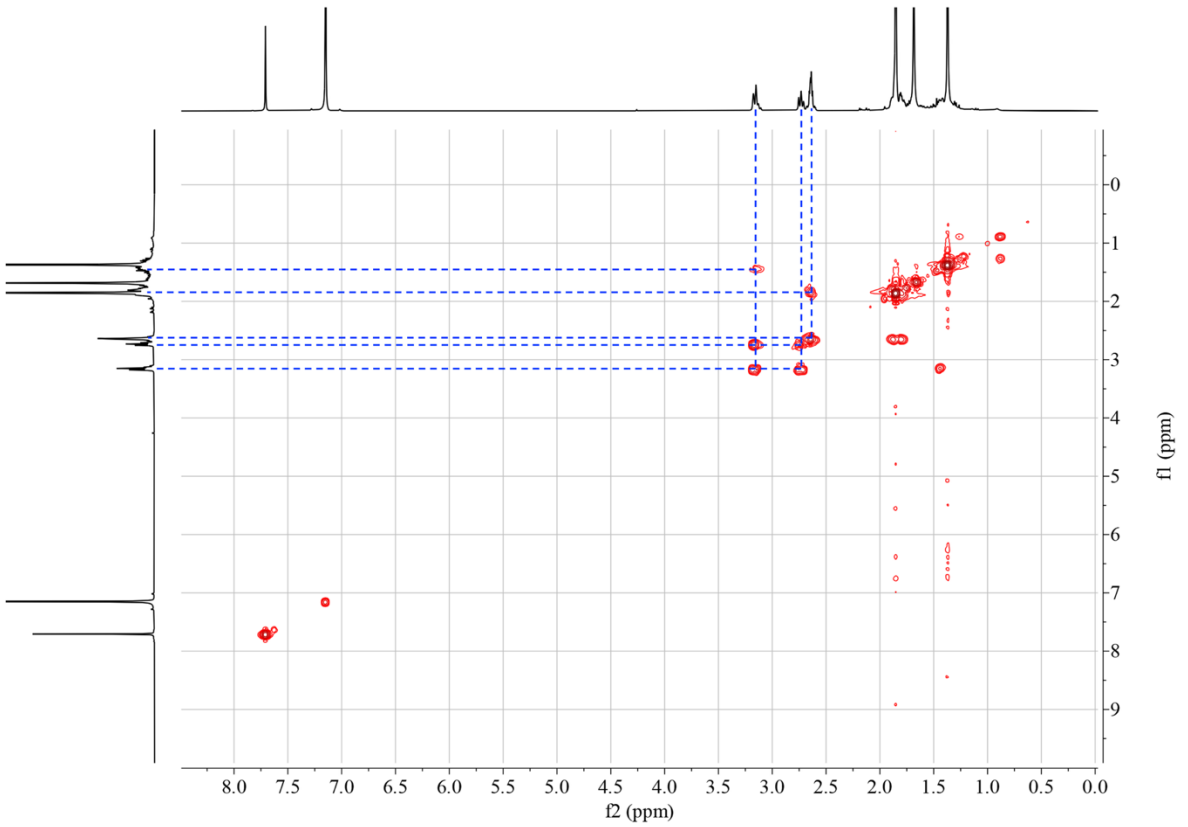

Figure S9. COSY NMR spectrum (600 MHz, C_6D_6, 30 °C) of complex **2b.**

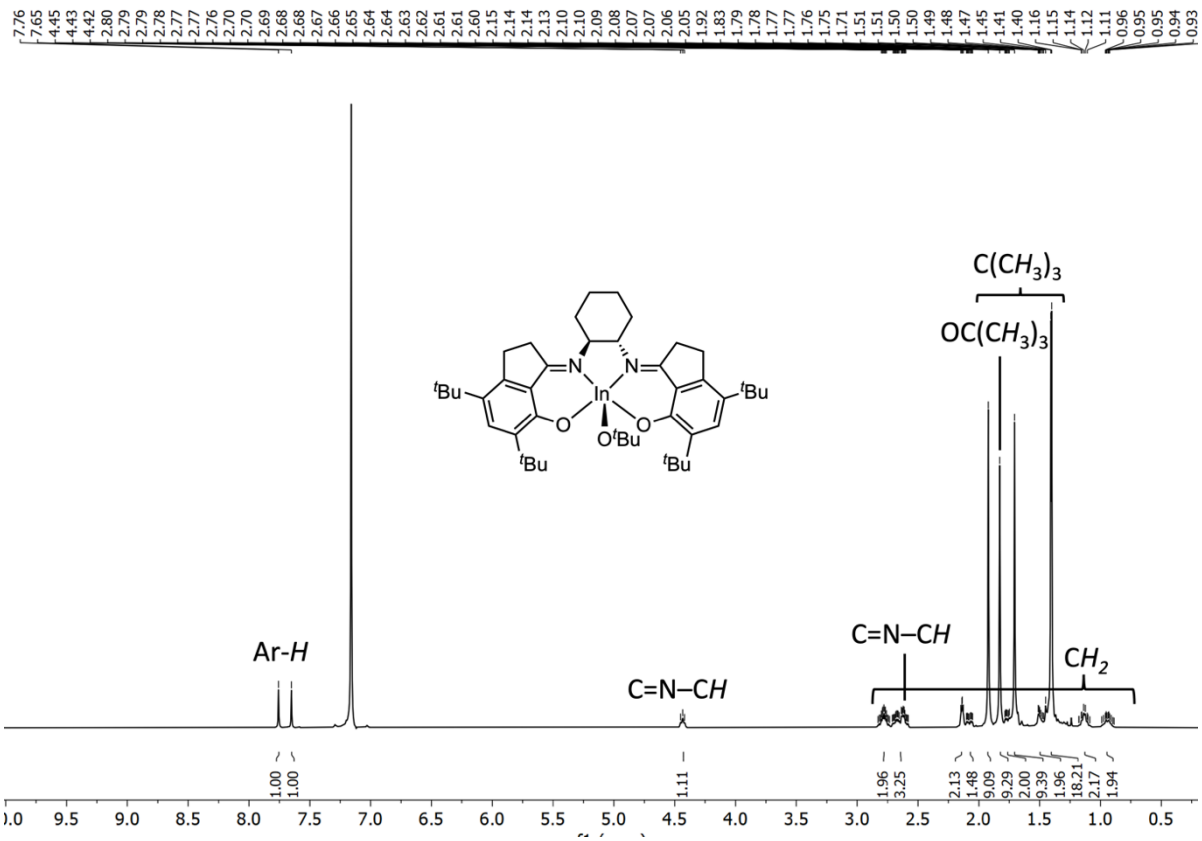

Figure S10. ^{1}H NMR spectrum (600 MHz, C_6D_6, 30 °C) of complex **2c.**

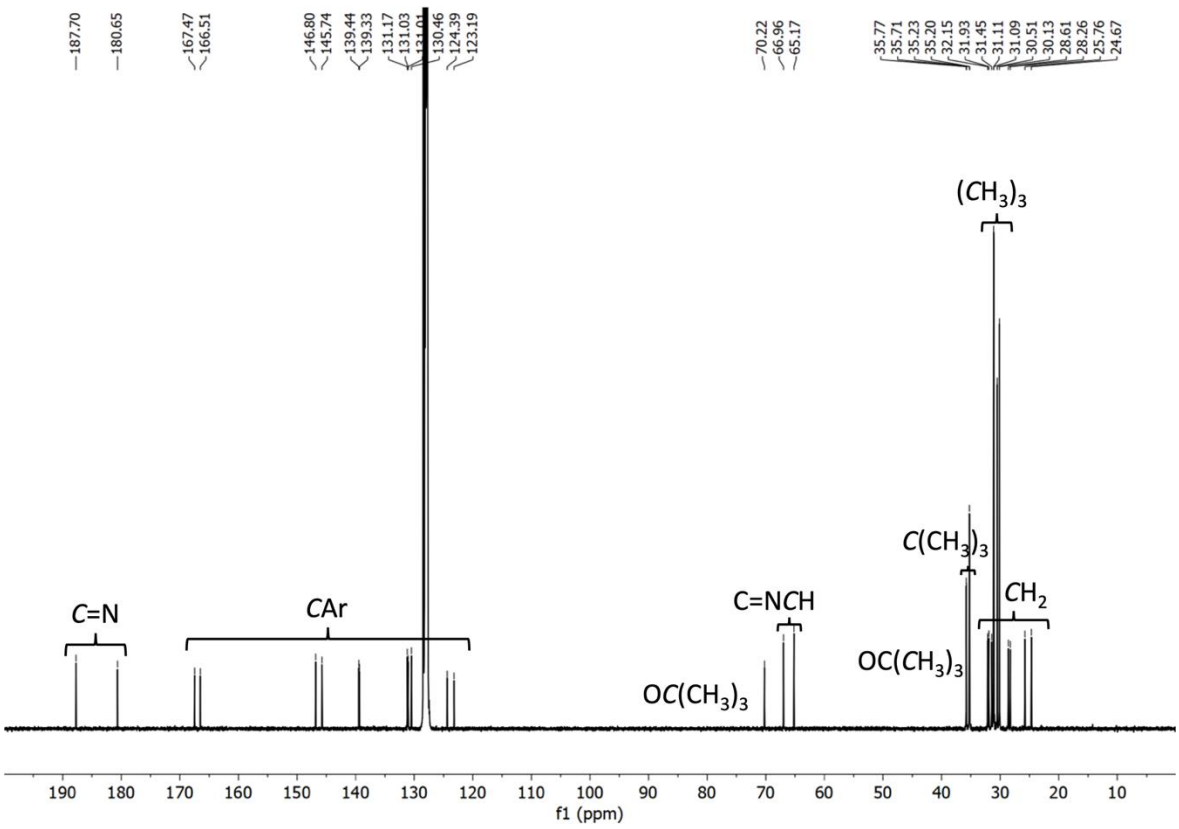

Figure S11. ^{13}C NMR spectrum (150 MHz, C_6D_6, 30 °C) of complex **2c**.

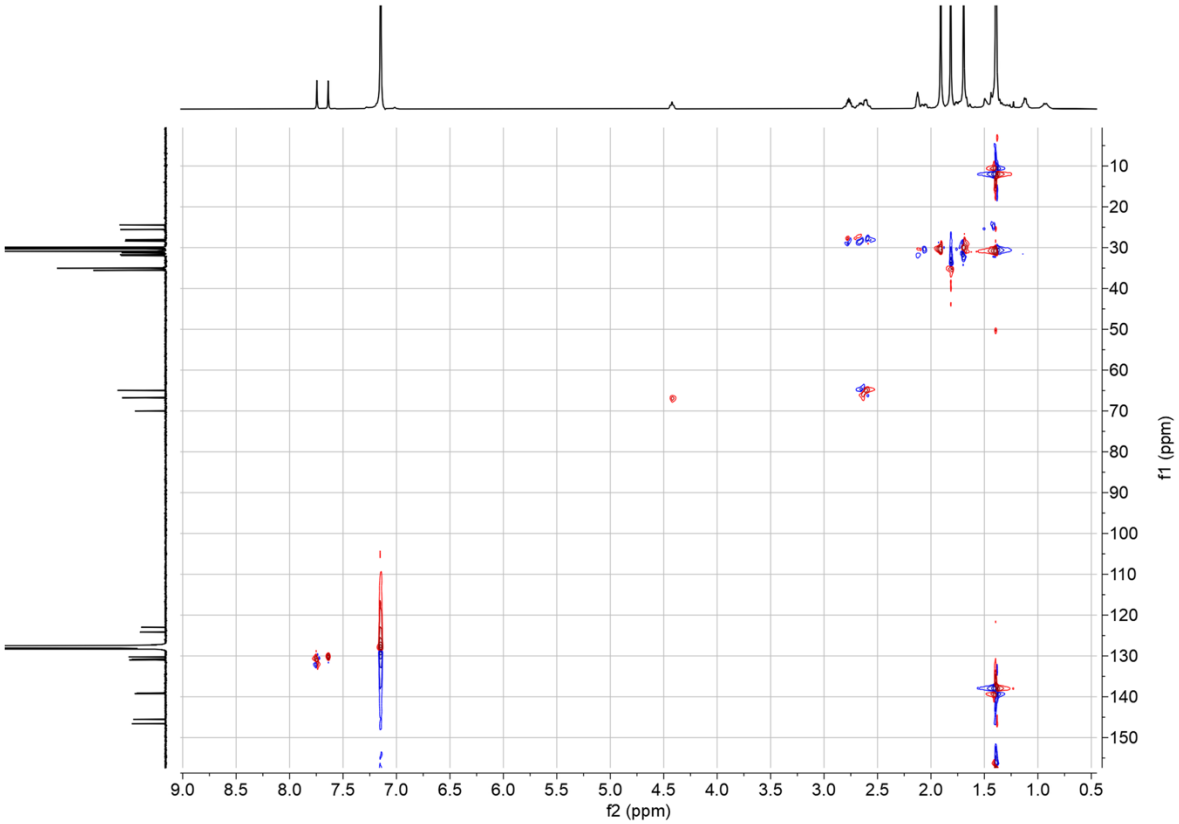

Figure S12. HSQC NMR spectrum (600 MHz, C_6D_6, 30 °C) of complex **2c.**

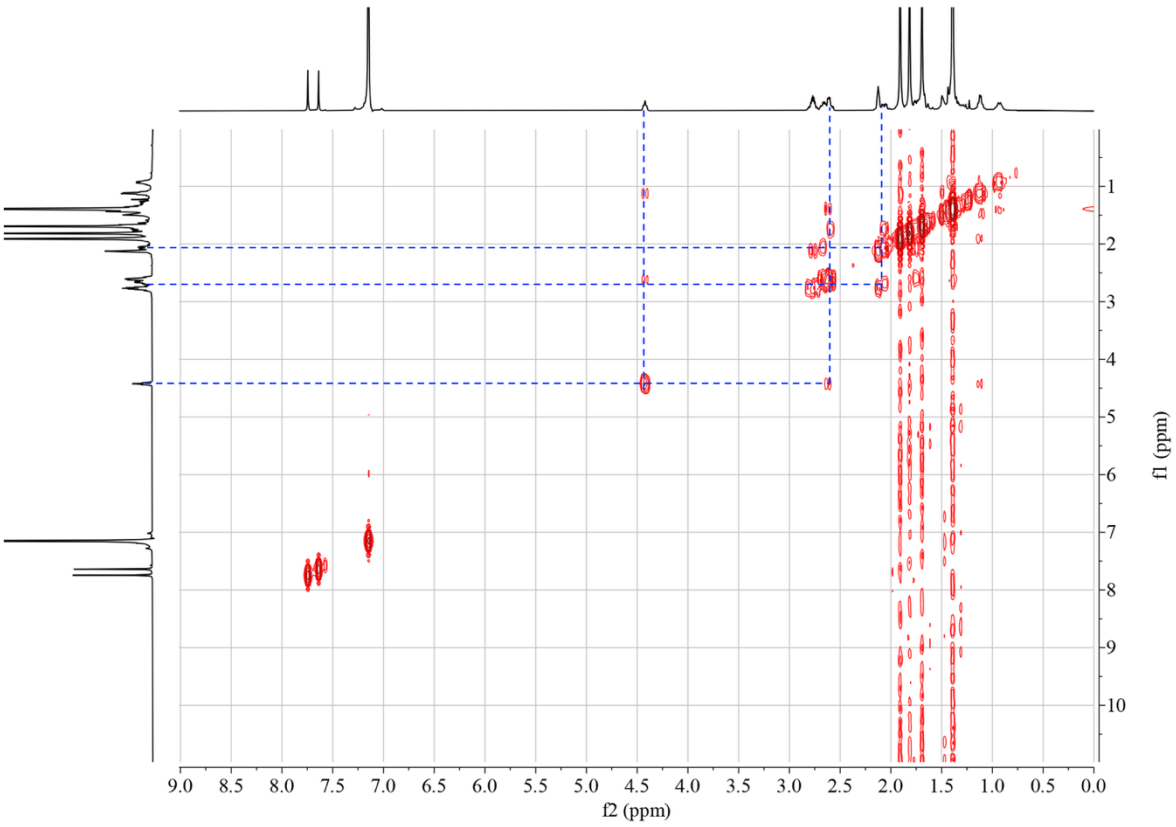

Figure S13. COSY NMR spectrum (600 MHz, C_6D_6, 30 °C) of complex **2c.**

Determination of P*r*LA tacticity

P*r*LA tacticity was determined from its ^{1}H NMR spectrum (Figure S7–S10). The spectra were deconvoluted using MestReNova. The P_m values was calculated from each of tetrad integrals using Bernoulli statistics equations as shown below:[1]

$$[rmr] = \frac{P_r^2}{2}$$

$$[rmm] = \frac{P_r P_m}{2}$$

$$[mmr] = \frac{P_r P_m}{2}$$

$$[mmm] = P_m^2 + \frac{P_r P_m}{2}$$

$$[mrm] = \frac{P_r^2 + P_r P_m}{2}$$

Tetrad	Integration	P_m
rmr	0.043	0.71
rmm	0.105	0.69
mmr	0.084	0.70
mmm	0.576	0.58
mrm	0.192	0.54
Average		0.64

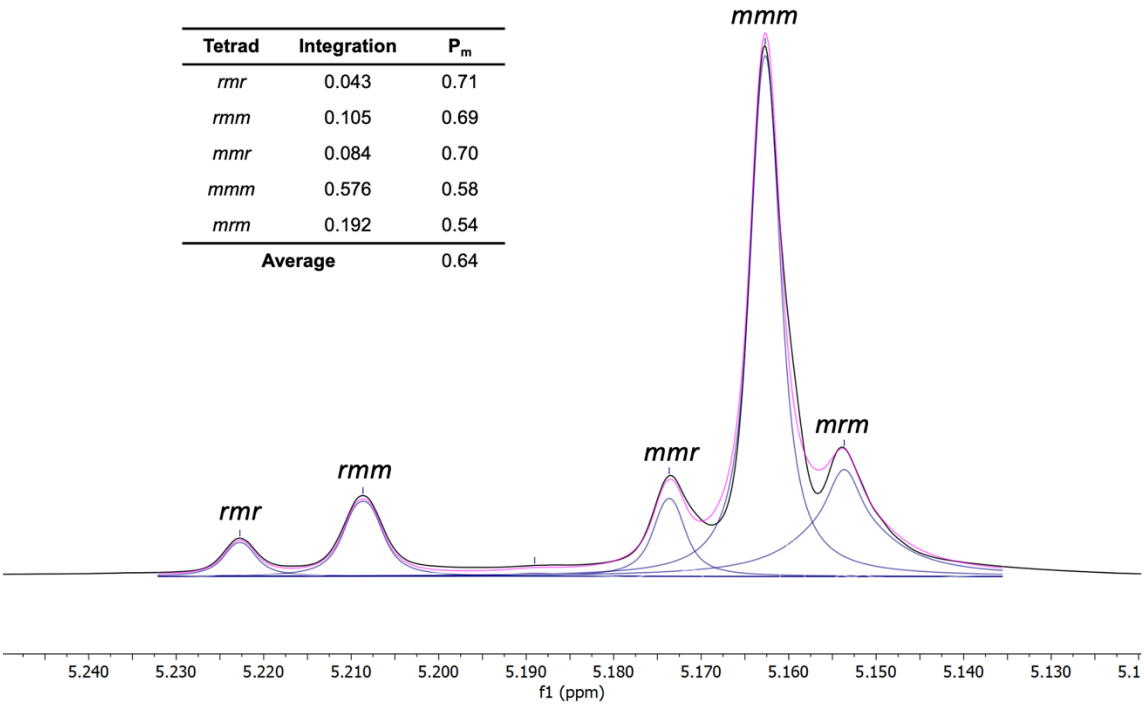

Figure S14. Homonuclear ^{1}H-decoupled NMR (600Hz, $CDCl_3$, 30 ºC) at methine region of poly(*rac*-LA) catalyzed by **2a** (Table 2., Entry 1).

Tetrad	Integration	P_m
rmr	0.032	0.75
rmm	0.087	0.72
mmr	0.093	0.72
mmm	0.605	0.56
mrm	0.184	0.57
Average		0.66

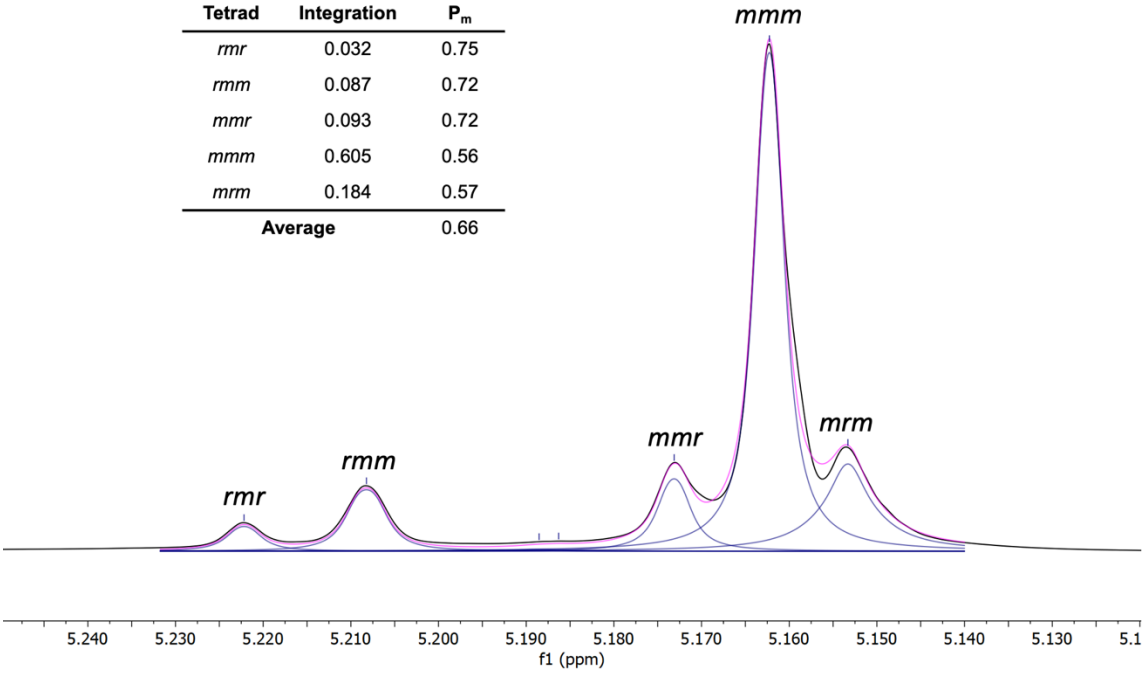

Figure S15. Homonuclear ^{1}H-decoupled NMR (600Hz, $CDCl_3$, 30 ºC) at methine region of poly(*rac*-LA) catalyzed by **2b** (Table 2., Entry 2).

Tetrad	Integration	P_m
rmr	0.027	0.77
rmm	0.076	0.76
mmr	0.104	0.75
mmm	0.664	0.68
mrm	0.128	0.78
Average		0.75

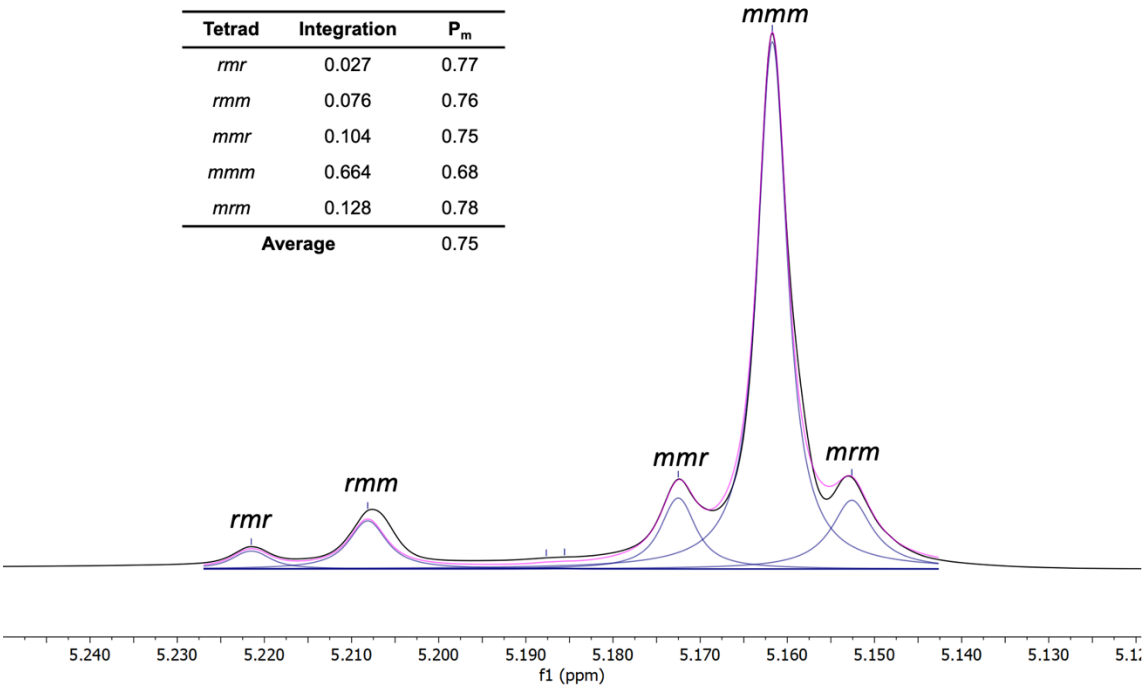

Figure S16. Homonuclear ^{1}H-decoupled NMR (600Hz, $CDCl_3$, 30 ºC) at methine region of poly(*rac*-LA) catalyzed by **2c** (Table 2., Entry 3).

Tetrad	Integration	P_m
rmr	0.009	0.87
rmm	0.065	0.87
mmr	0.063	0.87
mmm	0.818	0.81
mrm	0.046	0.82
Average		0.85

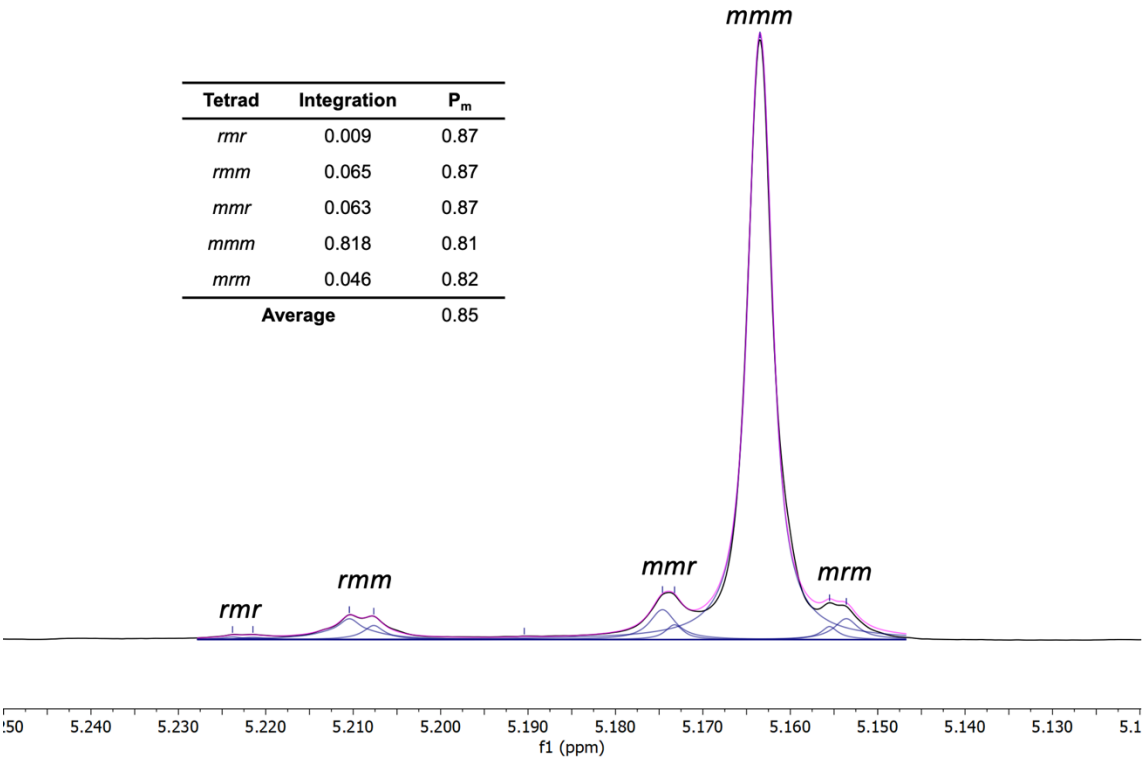

Figure S17. Homonuclear ^{1}H-decoupled NMR (600Hz, $CDCl_3$, 30 ºC) at methine region of poly(*rac*-LA) catalyzed by **2c** (Table 2., Entry 4).

End-group analysis

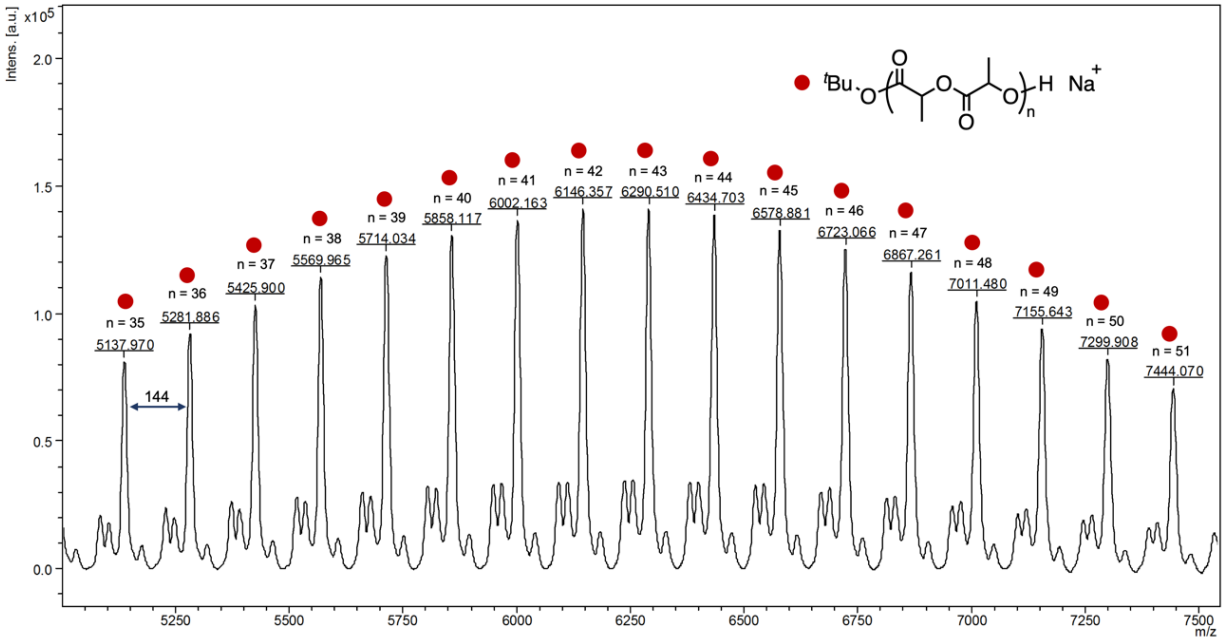

Figure S18. MALDI-TOF spectrum of PLA obtained from polymerization using 10:1 [*rac*-LA]:[**2c**], [*rac*-LA] = 0.50 M in DCM at room temperature for 1 min.

Kinetic analysis

The polymerizations of *rac*-LA, *L*-LA, *D*-LA or *ε*-CL was carried out in a glovebox with concentrations of monomer = 0.500 M in DCM and 200:1 of monomer to catalyst mole ratio. All experiments were carried out at room temperature and repeated three times. The aliquots of crude product were monitored by ^{1}H NMR spectroscopy to calculate a conversion. Then, the slope of three experiments were determined from the plot of $\ln([M]_0/[M]_t)$ vs reaction time. A plot of $\ln([M]_0/[M]_t)$ increased linearly with reaction time, indicating that the polymerization rate was first-order dependence on the monomer concentration. The polymerization rate: *rac*-LA ≈ *D*-LA > *L*-LA >> *ε*-CL.

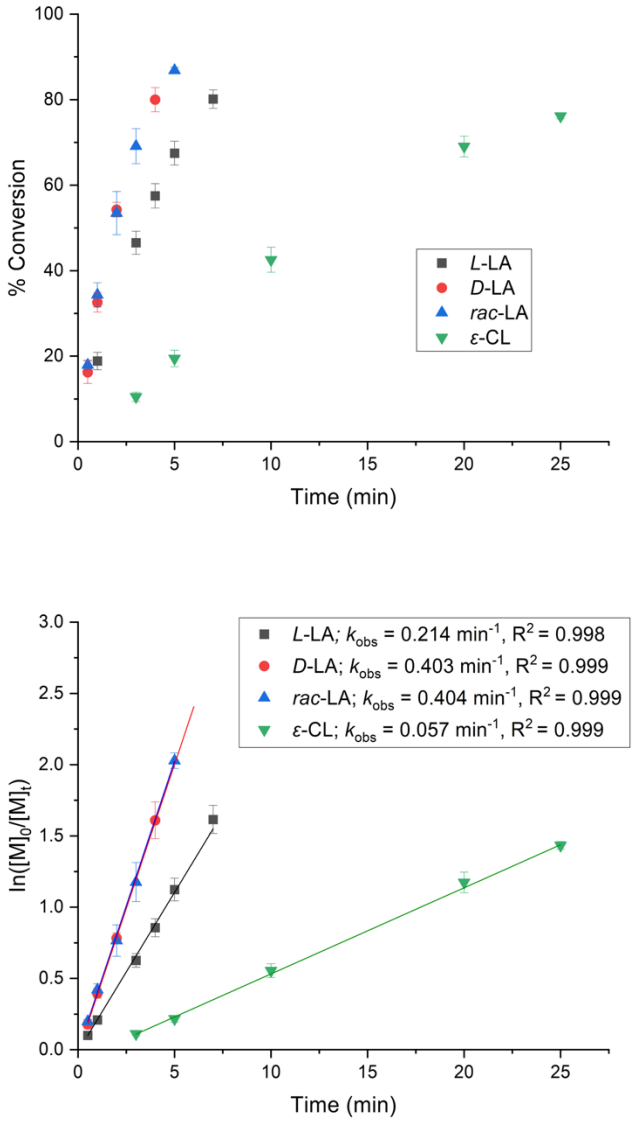

Figure S19. Polymerization of *L*-LA, *D*-LA, *rac*-LA, or ε-CL using [M]: [**2c**] = 200: 1and $[M]_0$ = 0.500 M in DCM, RT at different times. Plot of conversion with reaction time and (top) plot of $\ln([M]_0/[M]_t)$ vs reaction time (down).

Table S1 Ring-opening copolymerization (ROCOP) of *L*-LA and GA using complex **2c.**[a]

Entry	Monomer		[A]: [B]: [2c]	Time (min)	A Conv. (%)[b]	B Conv. (%)[b]	$M_{n,GPC}$ (kDa)[c]	$Đ$ [c]
	A	B						
1	*L*-LA	Ga	180: 20: 1	5	90	>99	97.8	1.27
2	*L*-LA	Ga	160: 40: 1	5	82	>99	81.2	1.38
3	*L*-LA	Ga	140: 60: 1	5	94	>99	-[d]	-[d]

[a] Reaction conditions: $[LA]_0$= 0.5 M, DCM, RT. [b] Conversion determined by ^{1}H NMR spectrum of crude polymer sample. [c] Determined by GPC analysis using a refractive index (RI) detector and polystyrene as a standard in THF. [d] Can't determine due to the solubility.

Calculation of the average monomer block lengths

The average lengths of lactyl blocks (L_{LA}) and glycolyl blocks (L_{GA}) can be calculated from the following equations:[2-5]

$$L_{LA} = \left(\frac{LL + LG}{LG}\right) \times 2$$

$$LL = [LLLL]$$

$$LG = [LLGG]$$

$$L_{GA} = \left(\frac{GG + GL}{GL}\right) \times 2$$

$$GG = [GGGG]$$

$$GL = [GGLL]$$

Note: Each LA monomer polymerizes into two L_{LA} units and each GA monomer polymerizes into two L_{GA} units.

The average lengths of lactyl blocks (L_{LA}) and caproyl blocks (L_{CL}) can be calculated from the following equation:[6, 7]

$$L_{LA} = \frac{\frac{1}{2}(LLL + LLC + CLL + CLC)}{CLC + \frac{1}{2}(LLC + CLL)}$$

$$LLL = \frac{1}{2}[CLLLL] + \frac{1}{2}[LLLLC] + \frac{1}{3}[CLLLC] + [LLLLLL]$$

$$LLC = \frac{1}{2}[CLLC] + \frac{1}{2}[LLLLC] + \frac{1}{3}[CLLLC]$$

$$CLL = \frac{1}{2}[CLLC] + \frac{1}{2}[CLLLL] + \frac{1}{3}[CLLLC]$$

$$CLC = [CLC]$$

$$L_{CL} = \frac{LCL + CCL + LCC + CCC}{LCL + \frac{1}{2}(CCL + LCC)}$$

$$LCL = [LLCLL] + [LLCLC] + [CLCLL] + [CLCLC]$$

$$CCL = [CCLC] + [CCLL]$$

$$LCC = [CLCC] + [LLCC]$$

$$CCC = [CCC]$$

Where [Seq.] are the contents of each sequence in the copolymer chain calculated from the integration of signals in the ^{13}C NMR spectrum of carbonyl region.

Note: Each LA monomer polymerizes into two L_{LA} units

Calculation of the reactivity ratio of monomer ($r_{monomer}$)

The reactivity ration of each monomer in copolymerization can be calculated from the following equation:[8, 9]

As the reactivity ratios follows Mayo-Lewis equation: $r_A = \frac{k_{AA}}{k_{AB}}$, $r_B = \frac{k_{BB}}{k_{BA}}$ (1)

where k_{ij} is the rate constant for adding monomer j to polymer ending with monomer i

The probability that polymer-ended monomer A adds monomer A is

$$P_{AA} = \frac{k_{AA}[M_A]}{k_{AA}[M_A] + k_{AB}[M_B]}$$

Then substitute eq. (1),

$$P_{AA} = \frac{r_A f_A}{r_A f_A + f_B} \qquad (2)$$

Where $f_A = \frac{[M_A]}{[M_A]+[M_B]}$ and $f_B = 1 - f_A$, f = the comonomer ratio

The average block length of monomer A follows the Bernoullian statistics:

$$L_A = \frac{1}{1 - P_{AA}}$$

So,

$$P_{AA} = 1 - \frac{1}{L_A} \qquad (3)$$

Substitute P_{AA} into the probability expression eq. (2) and (3)

$$1 - \frac{1}{L_A} = \frac{r_A f_A}{r_A f_A + f_B}$$

Rearrange to isolate r_A

$$r_A = \frac{(L_A \times f_B) - f_B}{f_A}$$

NMR spectra of copolymer

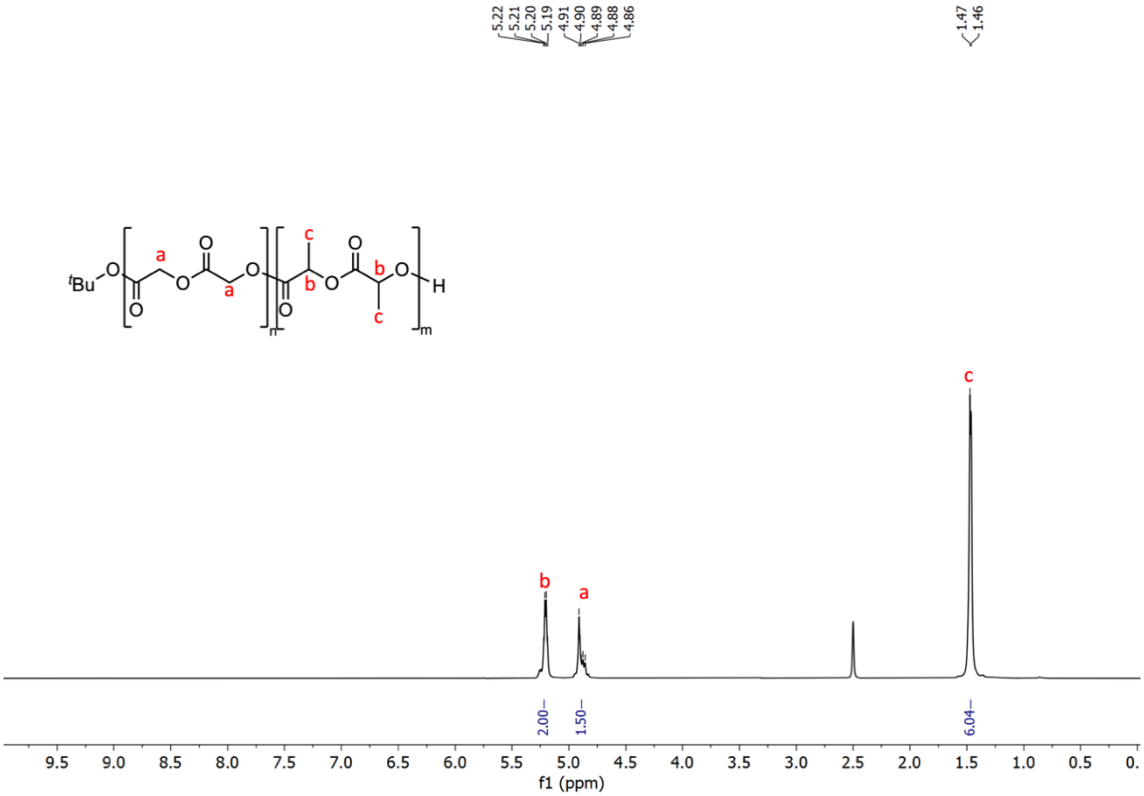

Figure S20. ^{1}H NMR spectrum (600 MHz, DMSO-d_6, 30 °C) of poly(*L*-LA-co-Ga) (Table 3, entry 1).

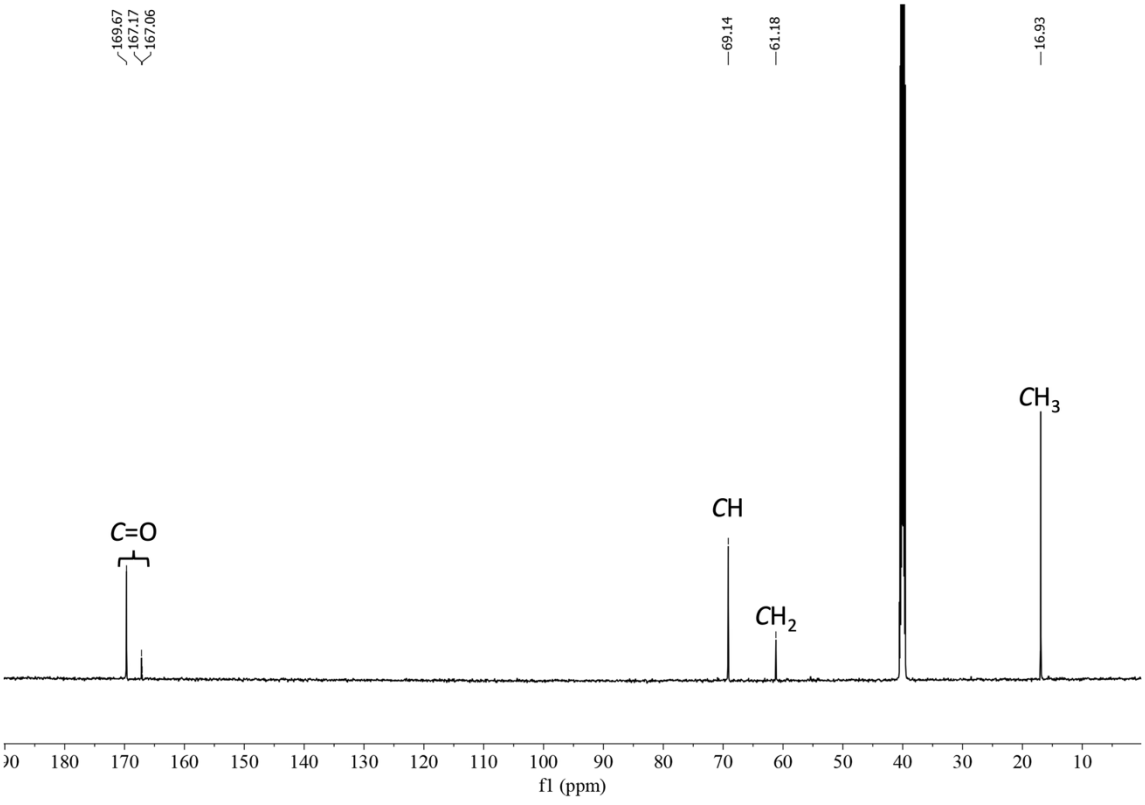

Figure S21. ^{13}C NMR spectrum (150 MHz, DMSO-d_6, 30 °C) of poly(*L*-LA-co-Ga) (Table 3, entry 1).

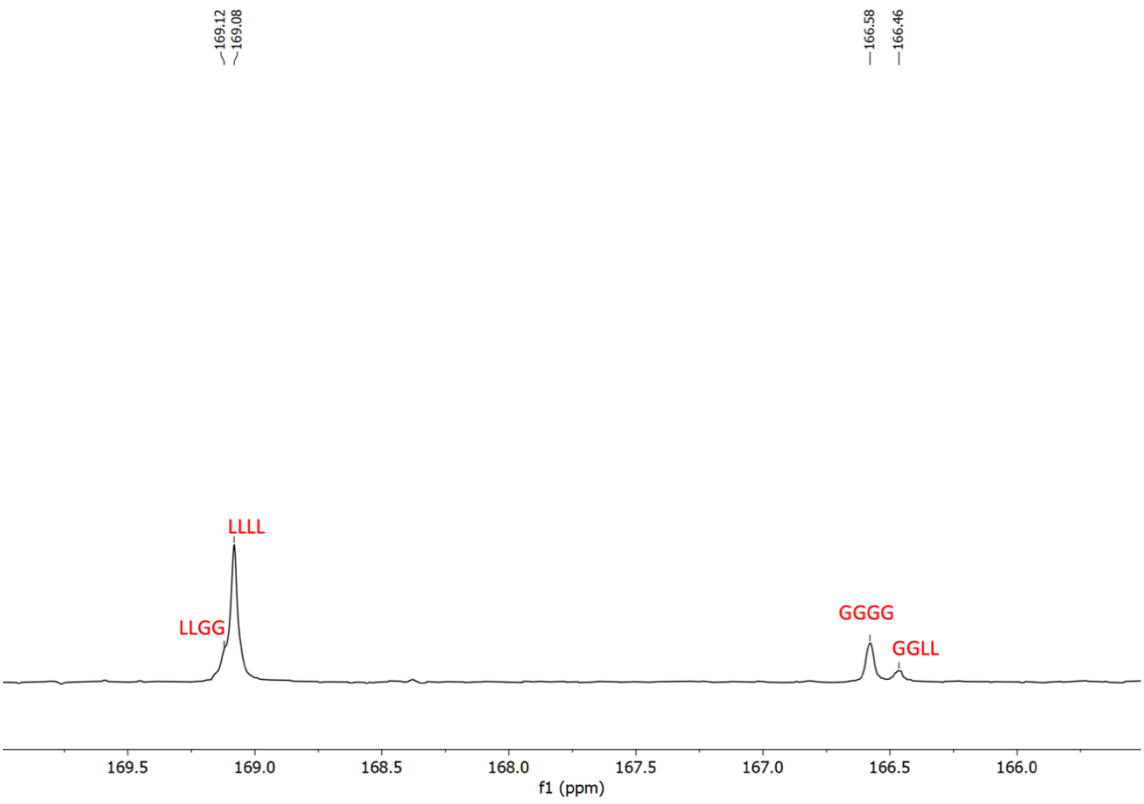

Figure S22. ^{13}C NMR spectrum (150 MHz, DMSO-d_6, 30 °C) of poly(*L*-LA-co-Ga) in carbonyl region (Table 3, entry 1).

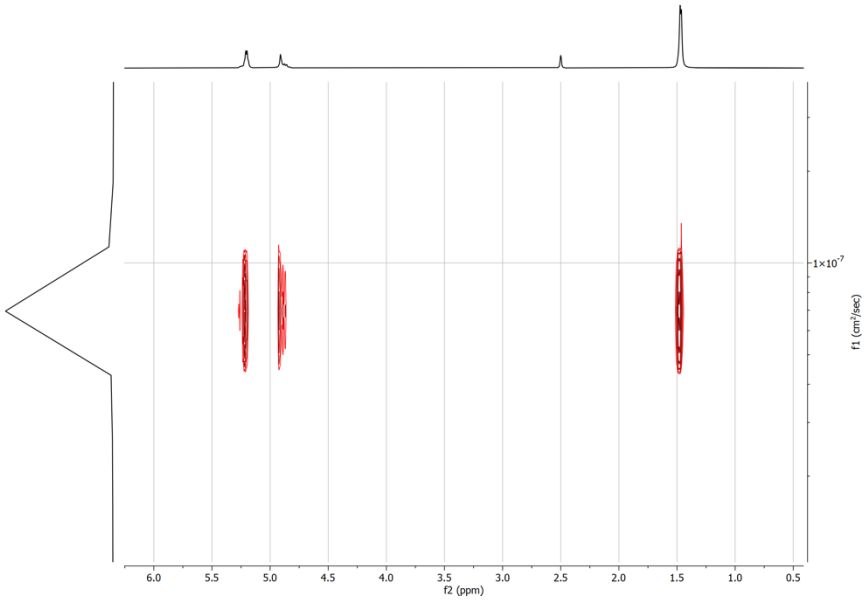

Figure S23. DOSY NMR spectrum (600 MHz, DMSO-d_6, 30 °C) of poly(*L*-LA-co-Ga) (Table 3, entry 1).

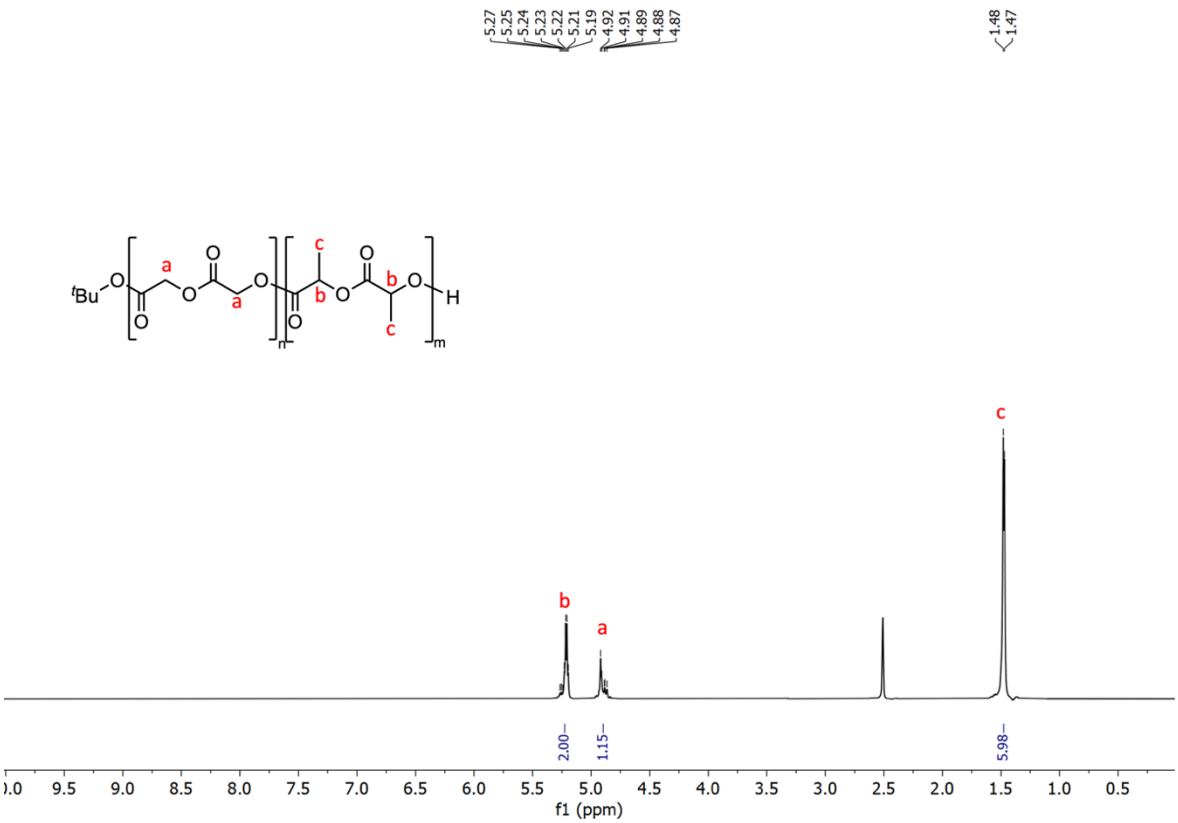

Figure S24. ^{1}H NMR spectrum (600 MHz, DMSO-d_6, 30 °C) of poly(*D*-LA-co-Ga) (Table 3, entry 2).

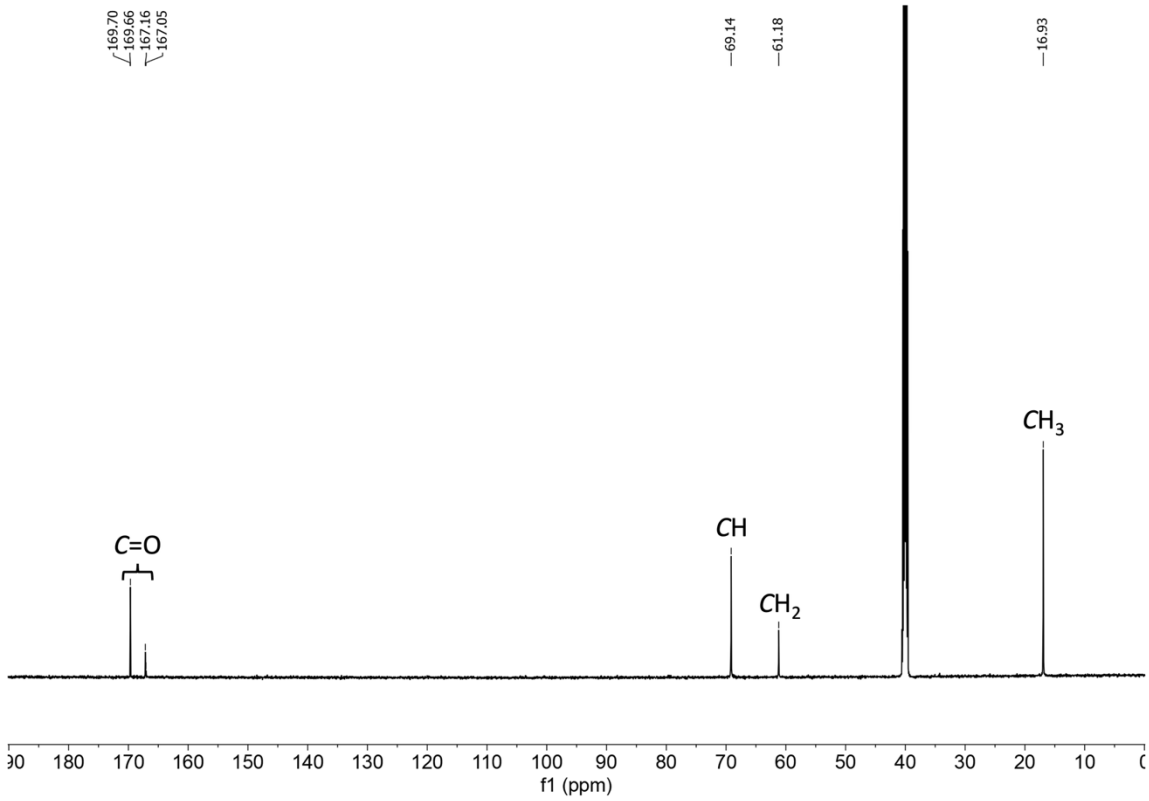

Figure S25. ^{13}C NMR spectrum (150 MHz, DMSO-d_6, 30 °C) of poly(*D*-LA-co-Ga) (Table 3, entry 2).

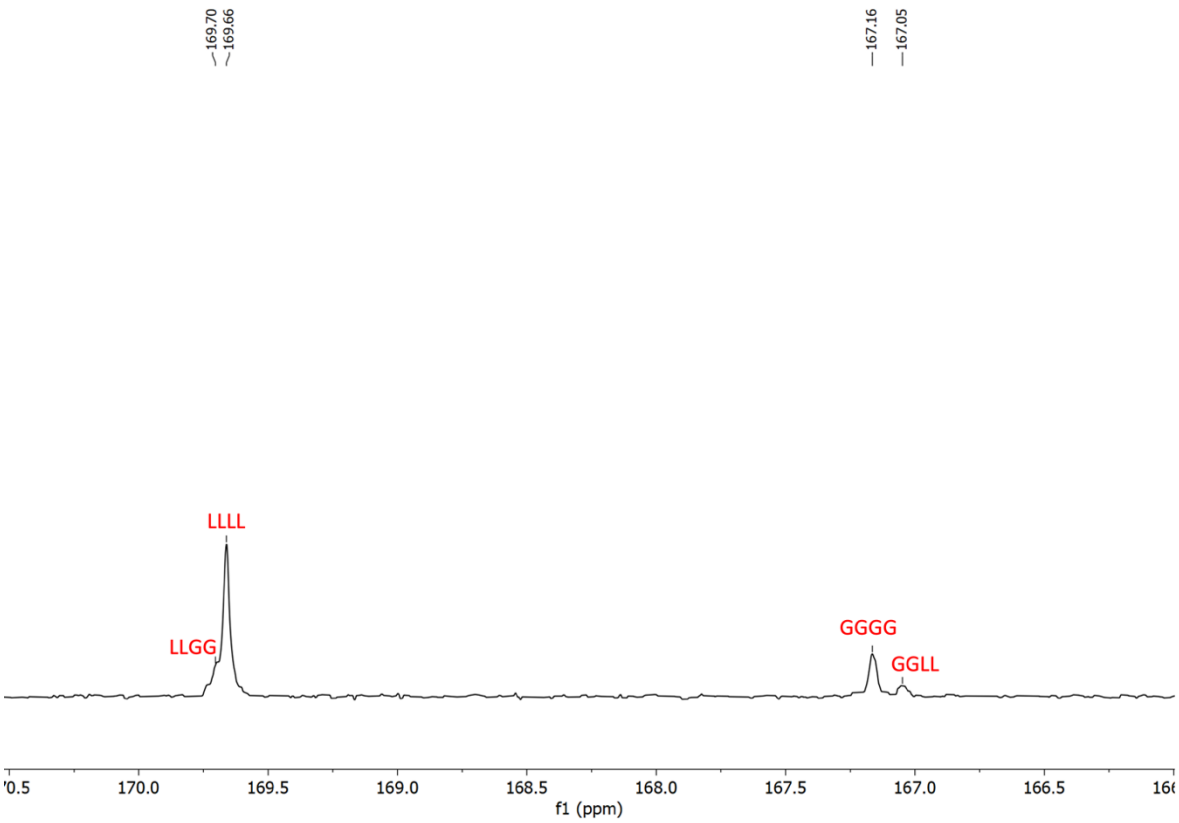

Figure S26. ^{13}C NMR spectrum (150 MHz, DMSO-d_6, 30 °C) of poly(*D*-LA-co-Ga) in carbonyl region (Table 3, entry 2).

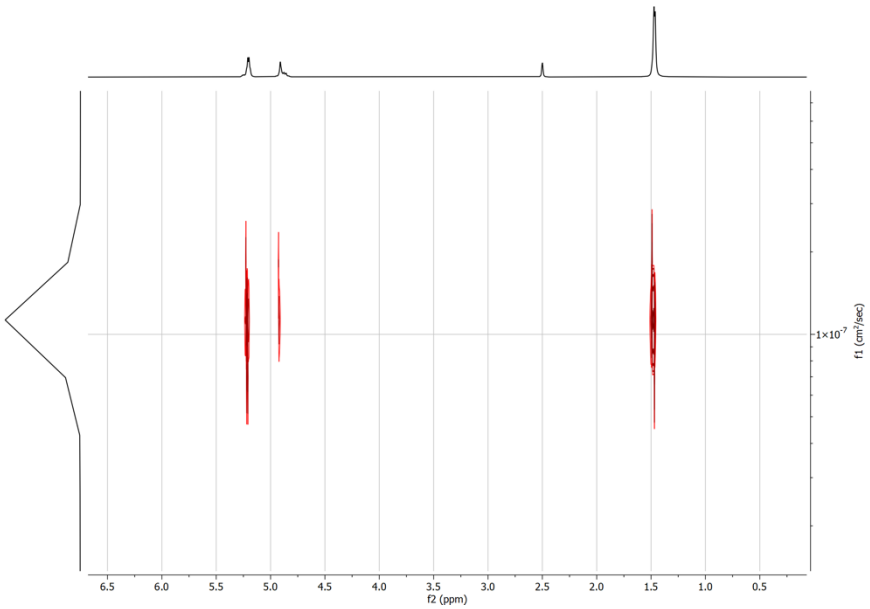

Figure S27. DOSY NMR spectrum (600 MHz, DMSO-d_6, 30 °C) of poly(*D*-LA-co-Ga) (Table 3, entry 2).

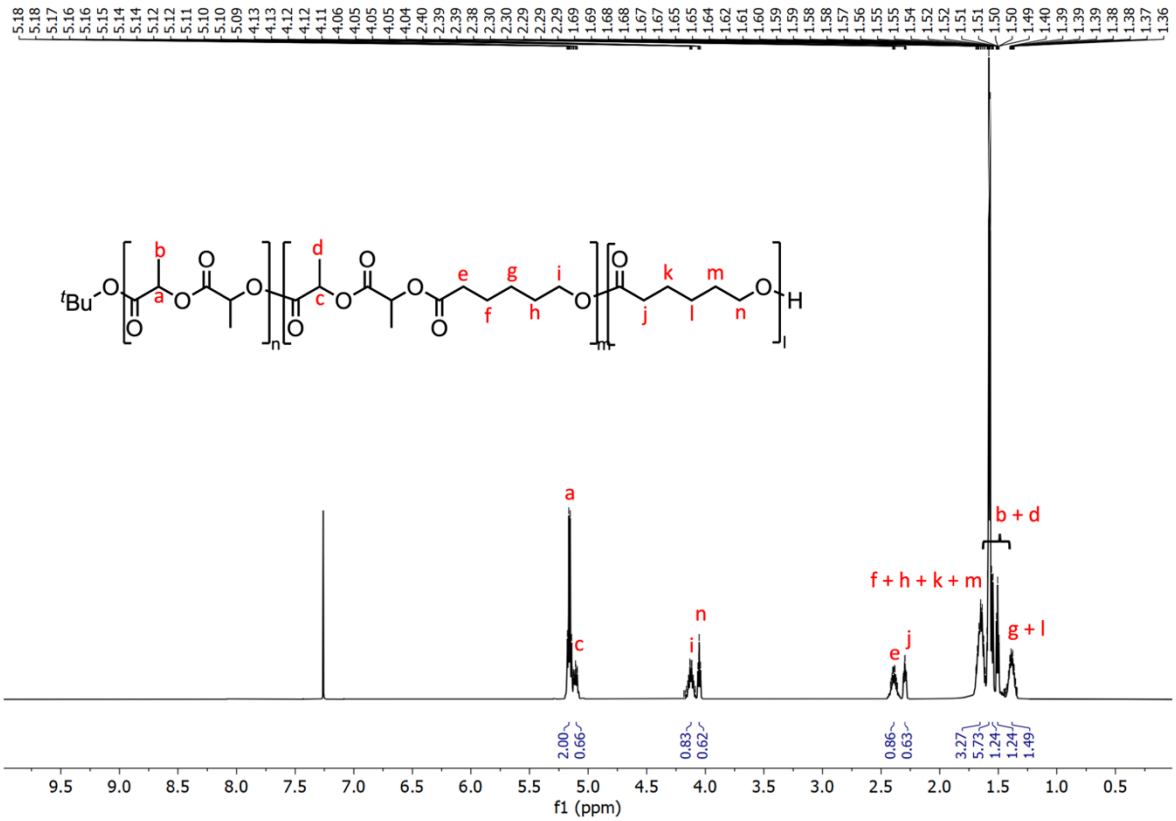

Figure S28. ^{1}H NMR spectrum (600 MHz, $CDCl_3$, 30 °C) of poly(*L*-LA -co-*Ɛ*-CL) (Table 3, entry 3).

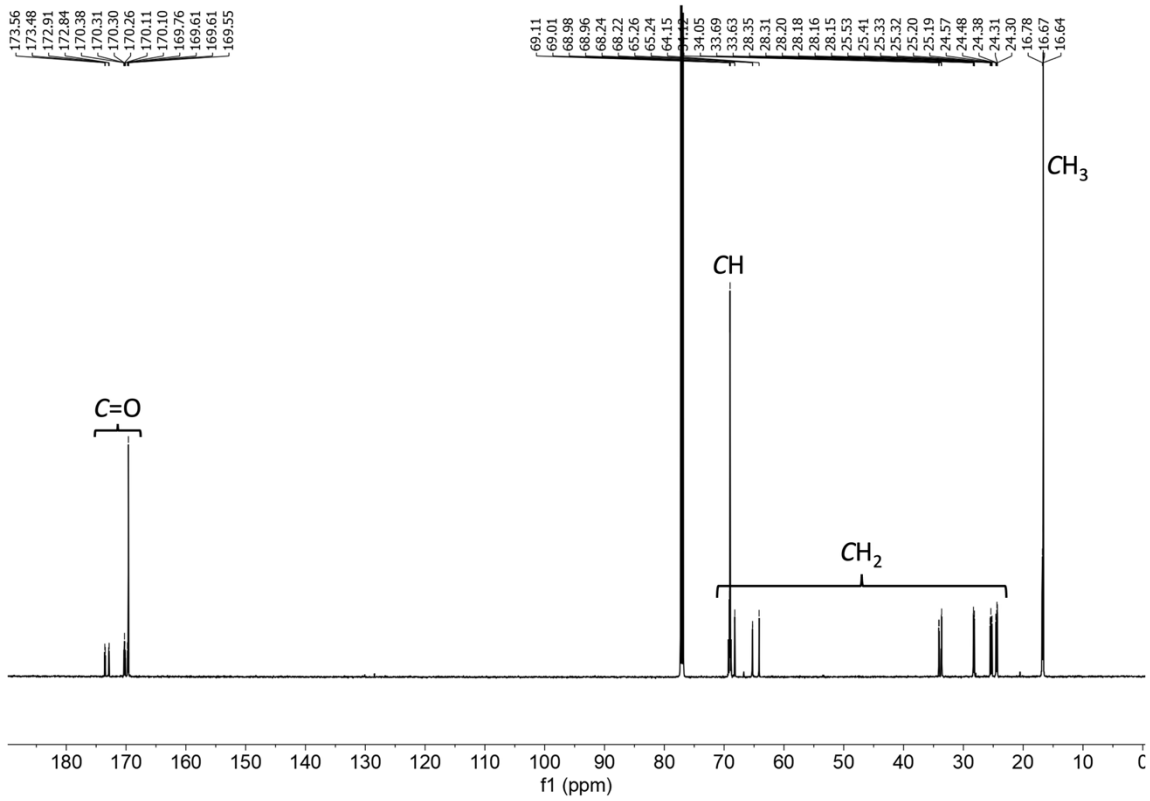

Figure S29. ^{13}C NMR spectrum (150 MHz, $CDCl_3$, 30 °C) of poly (*L*-LA -co-*Ɛ*-CL) (Table 3, entry 3).

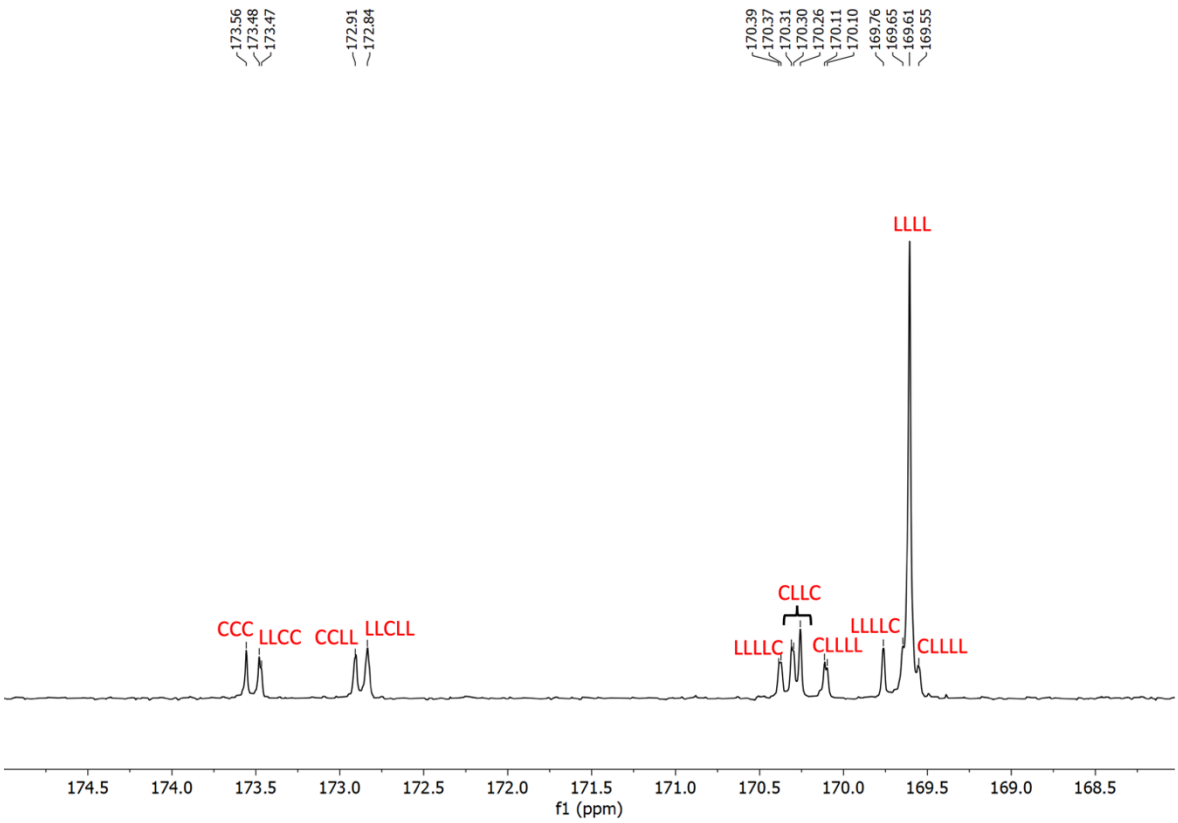

Figure S30. ^{13}C NMR spectrum (150 MHz, $CDCl_3$, 30 °C) of poly(*L*-LA -co-*Ɛ*-CL) in carbonyl region (Table 3, entry 3).

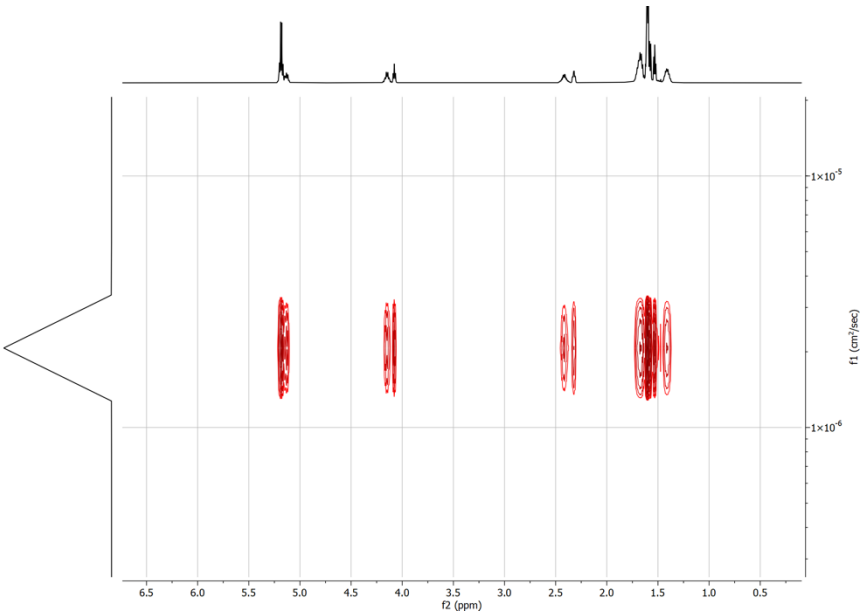

Figure S31. DOSY NMR spectrum (600 MHz, $CDCl_3$, 30 °C) of poly(*L*-LA -co-*Ɛ*-CL) (Table 3, entry 3).

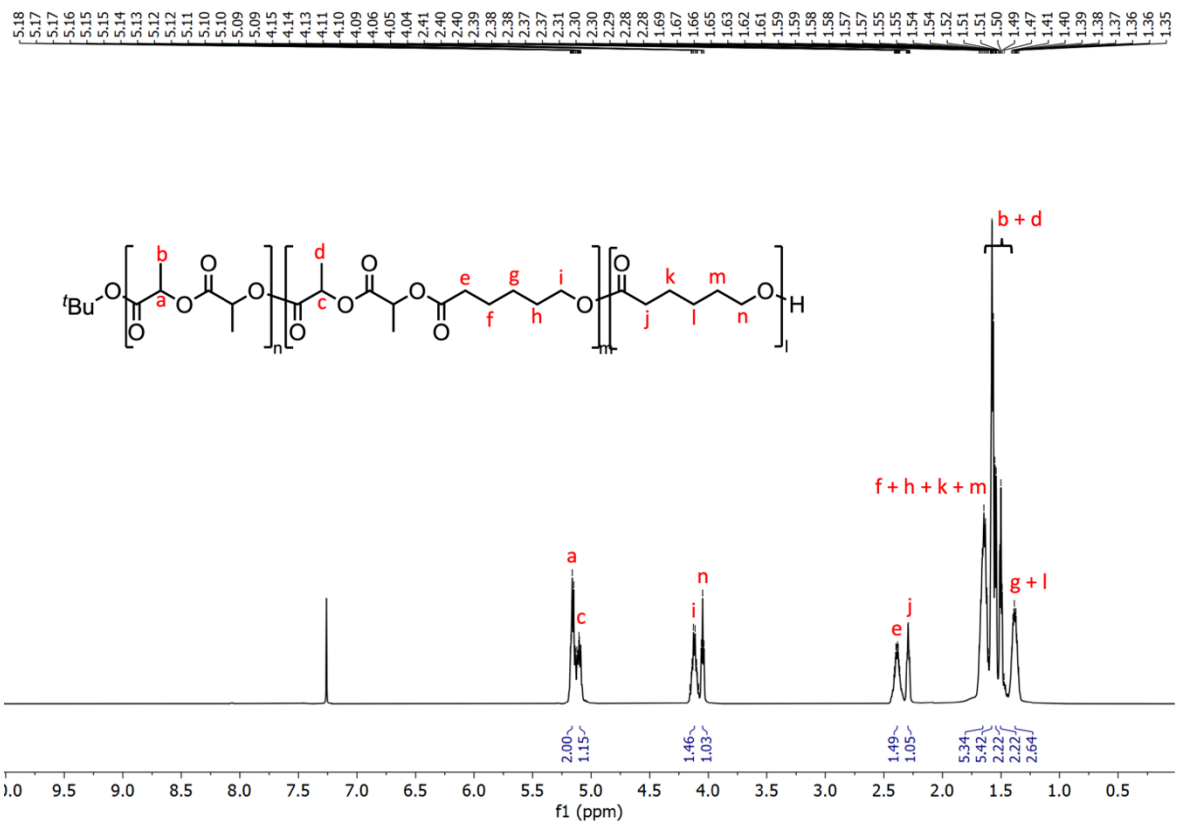

Figure S32. ^{1}H NMR spectrum (600 MHz, $CDCl_3$, 30 °C) of poly(*D*-LA -co-*Ɛ*-CL) (Table 3, entry 4).

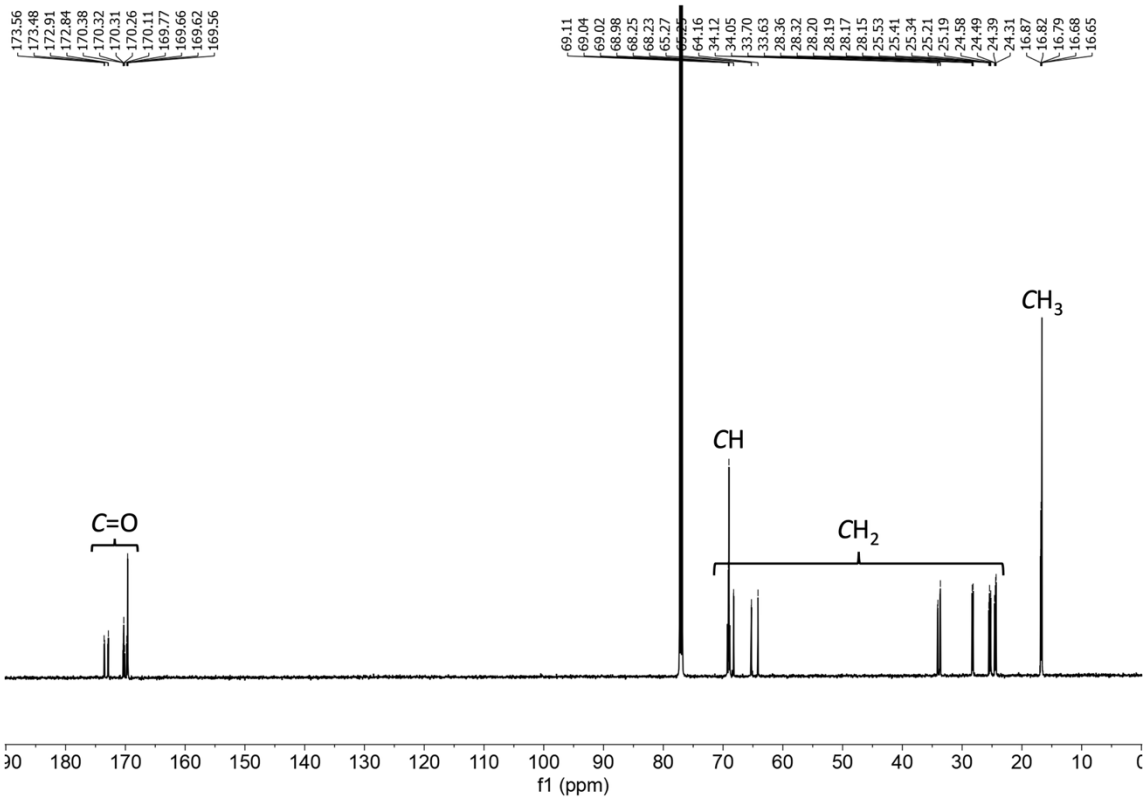

Figure S33. ^{13}C NMR spectrum (150 MHz, $CDCl_3$, 30 °C) of poly(*D*-LA -co-*Ɛ*-CL) (Table 3, entry 4).

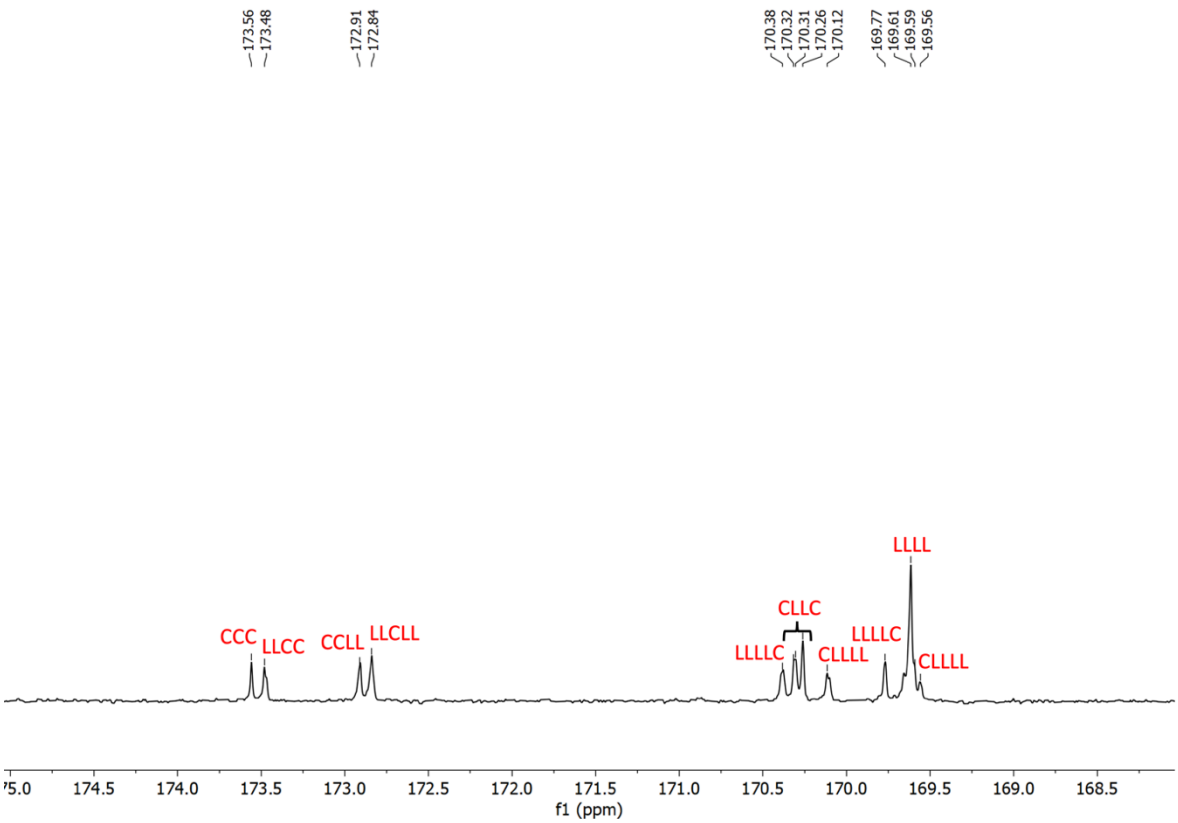

Figure S34. ^{13}C NMR spectrum (150 MHz, $CDCl_3$, 30 °C) of poly(*D*-LA -co-*Ɛ*-CL) in carbonyl region (Table 3, entry 4).

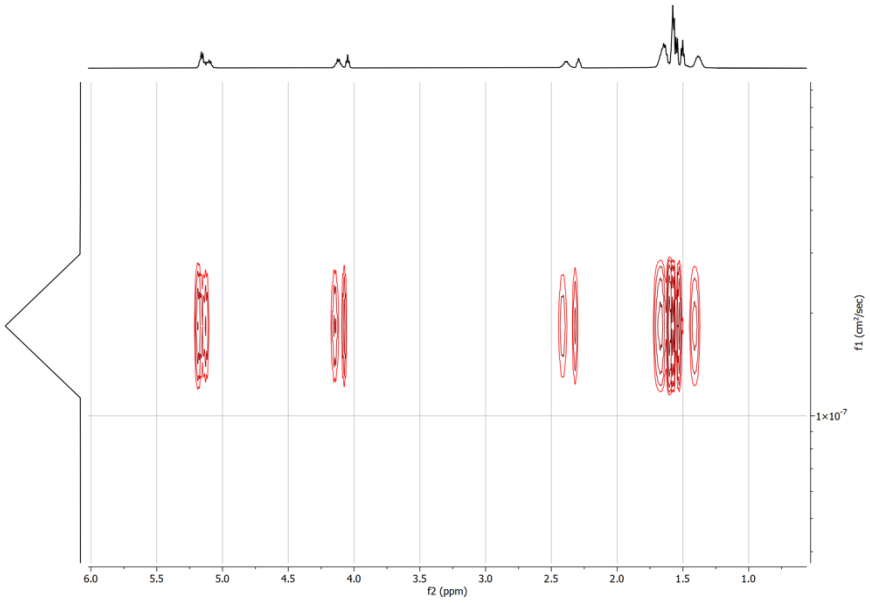

Figure S35. DOSY NMR spectrum (600 MHz, $CDCl_3$, 30 °C) of poly(*D*-LA -co-*Ɛ*-CL) (Table 3, entry 4).

GPC profile of polymers

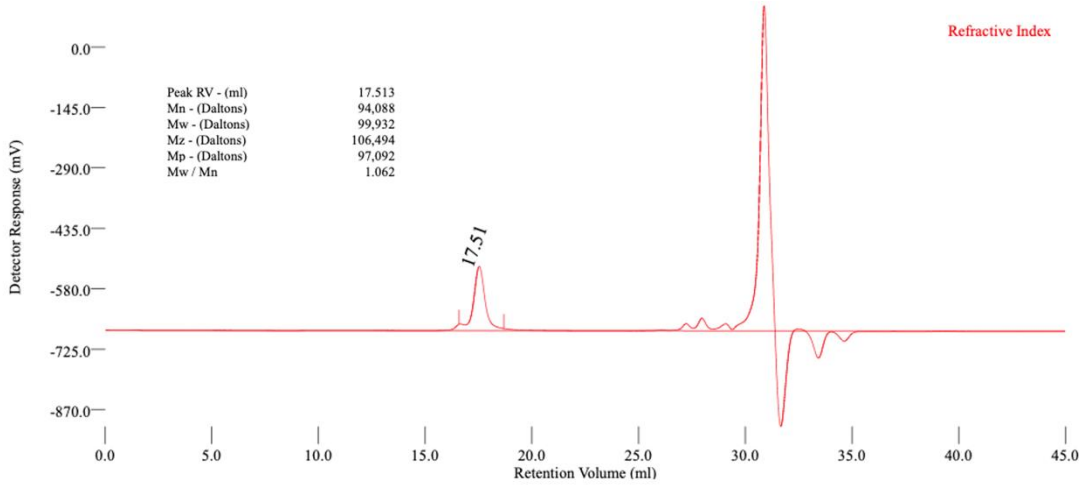

Figure S36. GPC traces of poly (*L*-LA) (Table 1, entry 1).

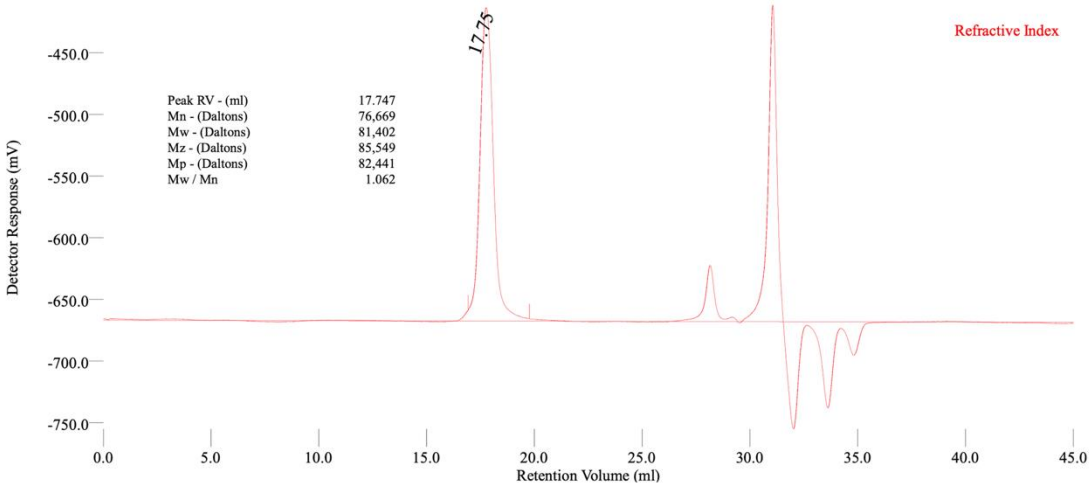

Figure S37. GPC traces of poly (*L*-LA) (Table 1, entry 2).

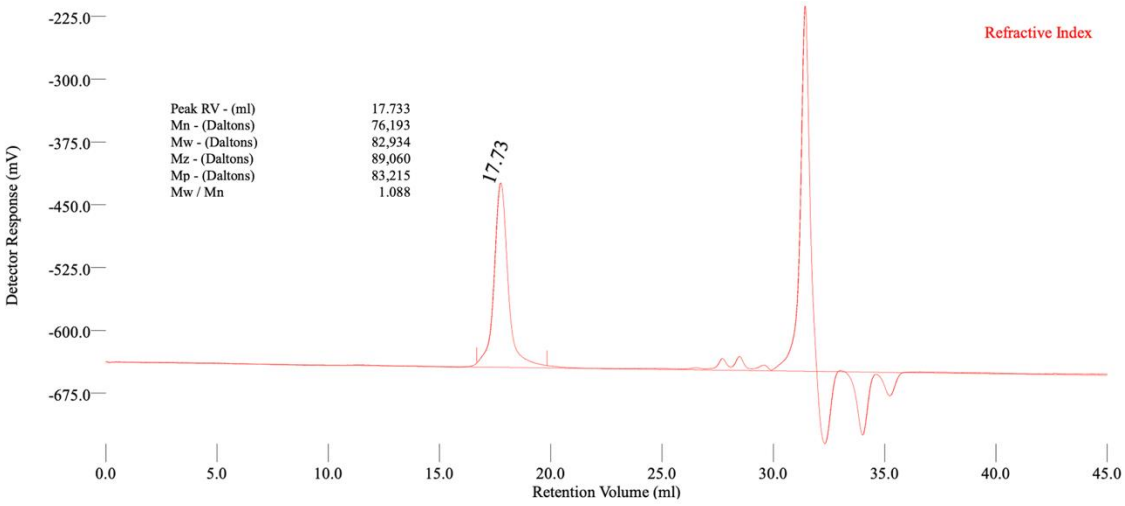

Figure S38. GPC traces of poly (*L*-LA) (Table 1, entry 3).

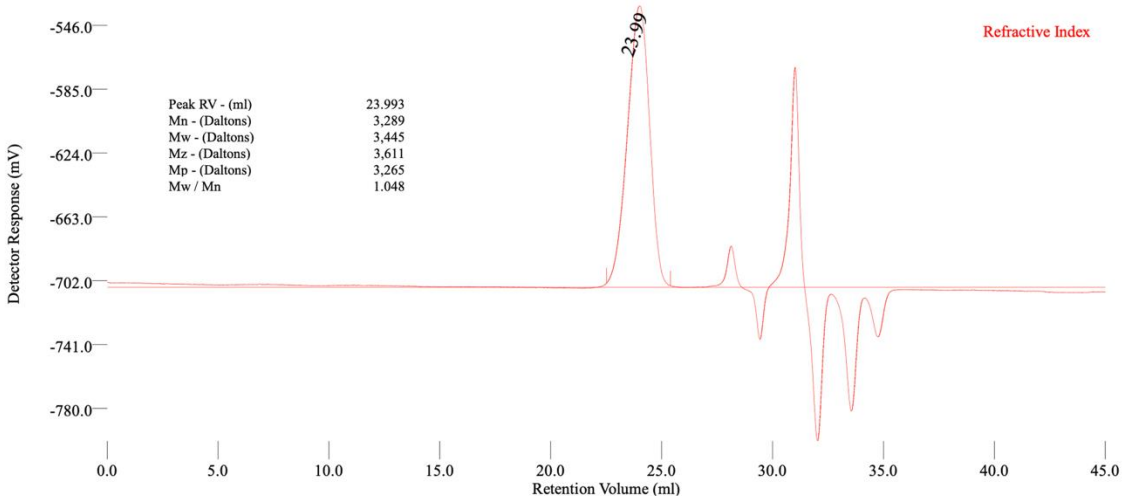

Figure S39. GPC traces of poly (*L*-LA) (Table 1, entry 4).

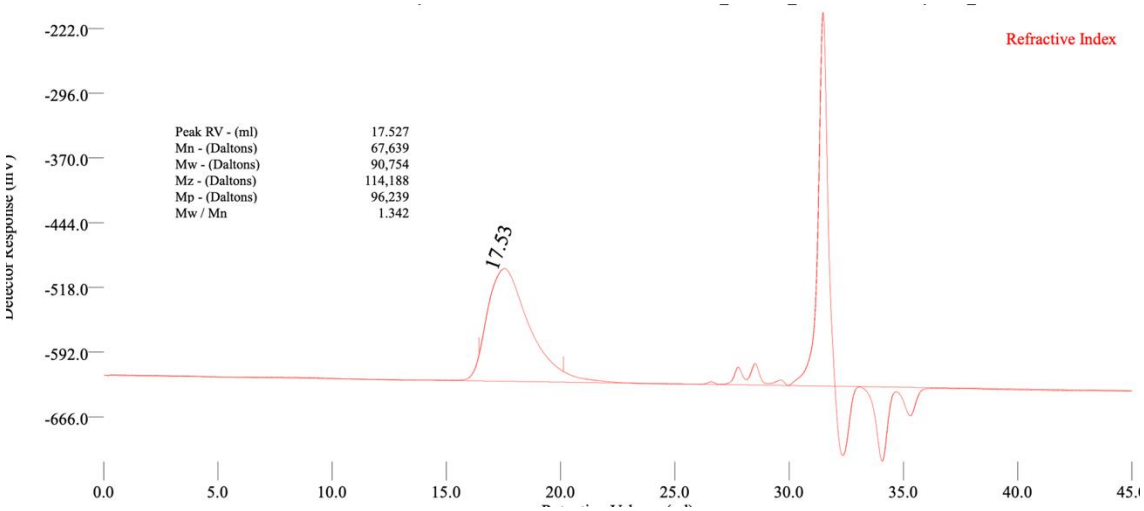

Figure S40. GPC traces of poly (*ε*-CL) (Table 1, entry 7).

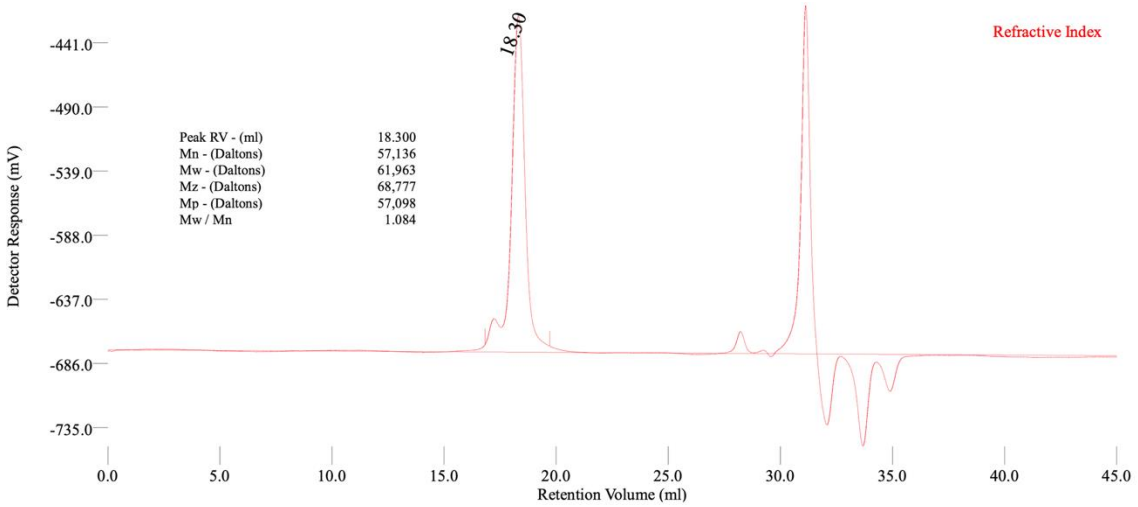

Figure S41. GPC traces of poly (*rac*-LA) (Table 2, entry 1).

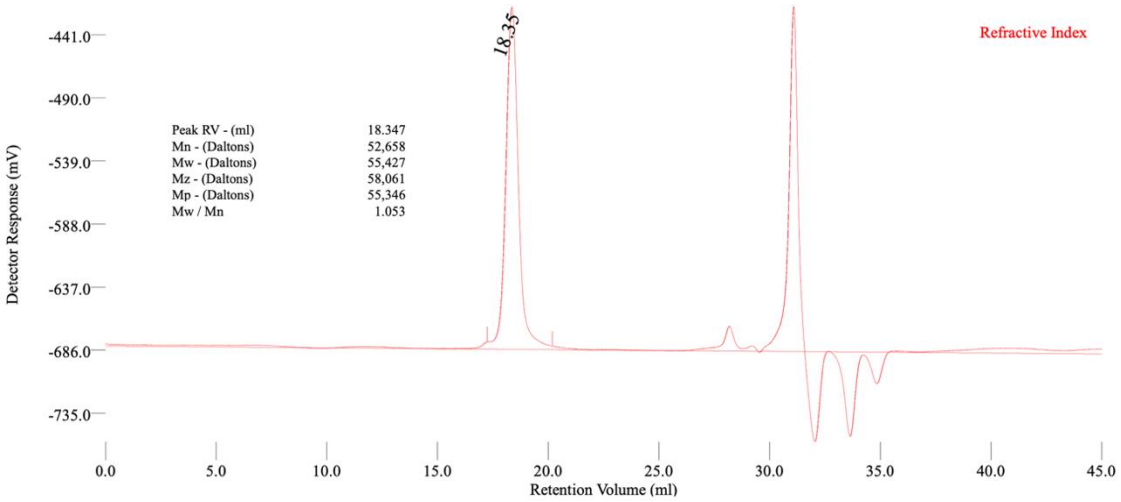

Figure S42. GPC traces of poly (*rac*-LA) (Table 2, entry 2).

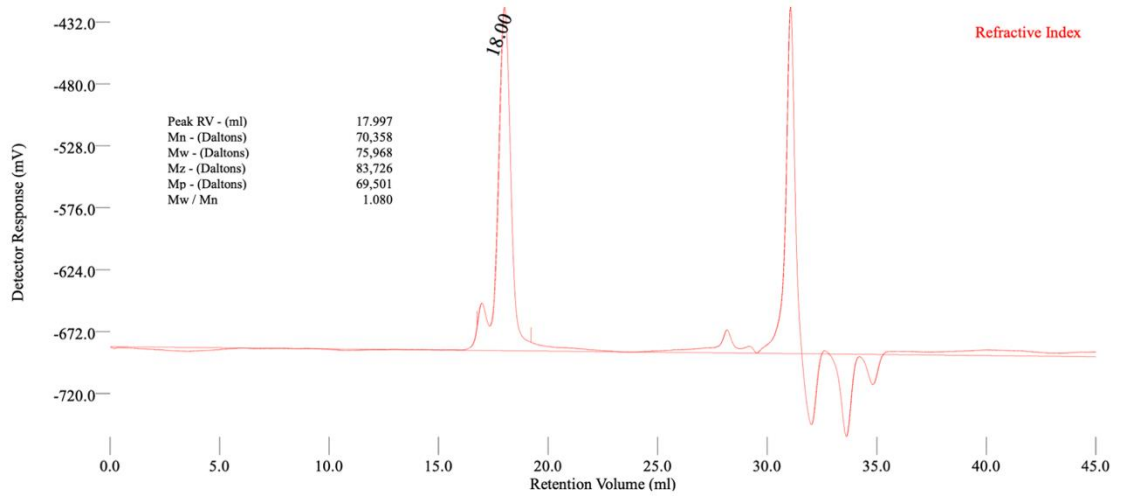

Figure S43. GPC traces of poly (*rac*-LA) (Table 2, entry 3).

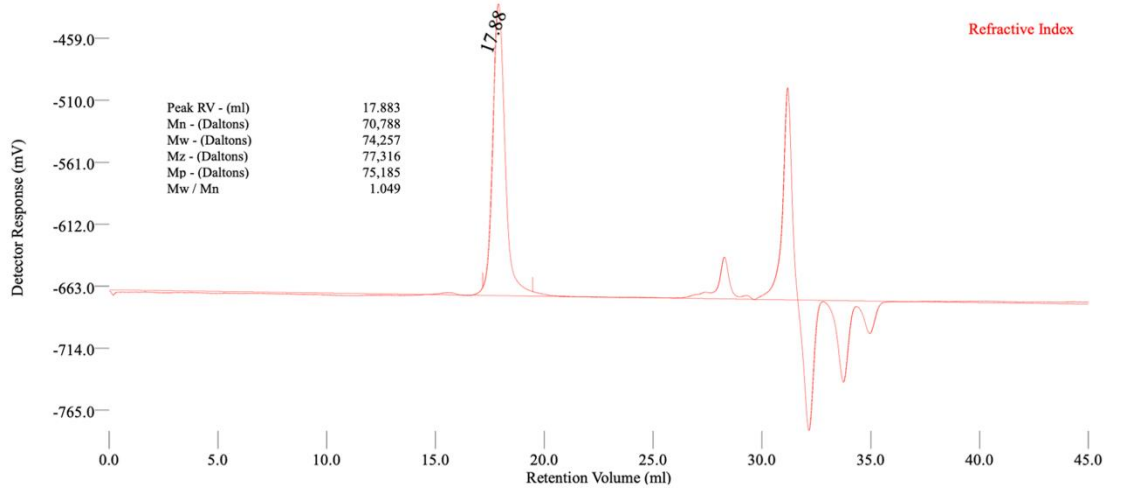

Figure S44. GPC traces of poly (*rac*-LA) (Table 2, entry 4).

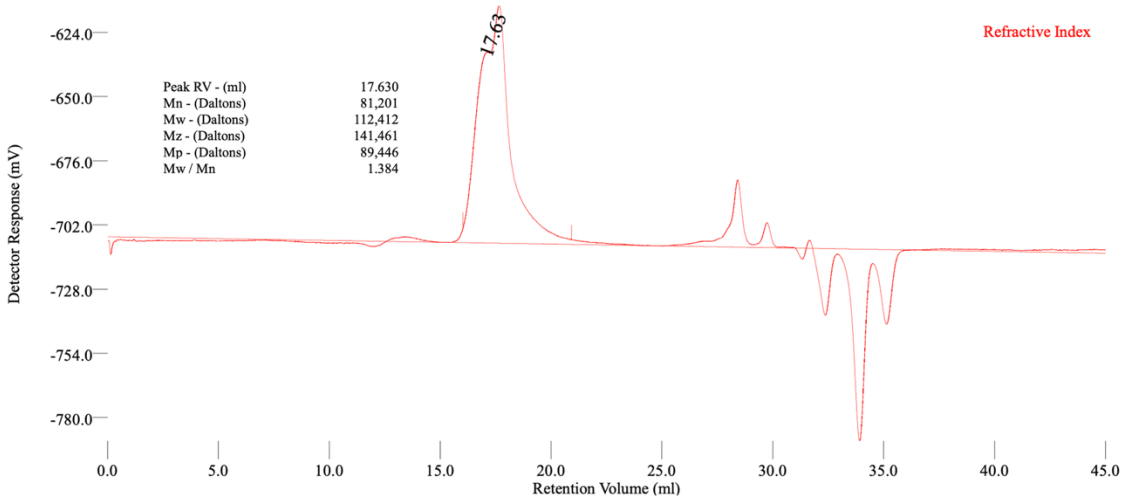

Figure S45. GPC traces of poly (*L*-LA -*co*- GA) (Table 3, entry 1).

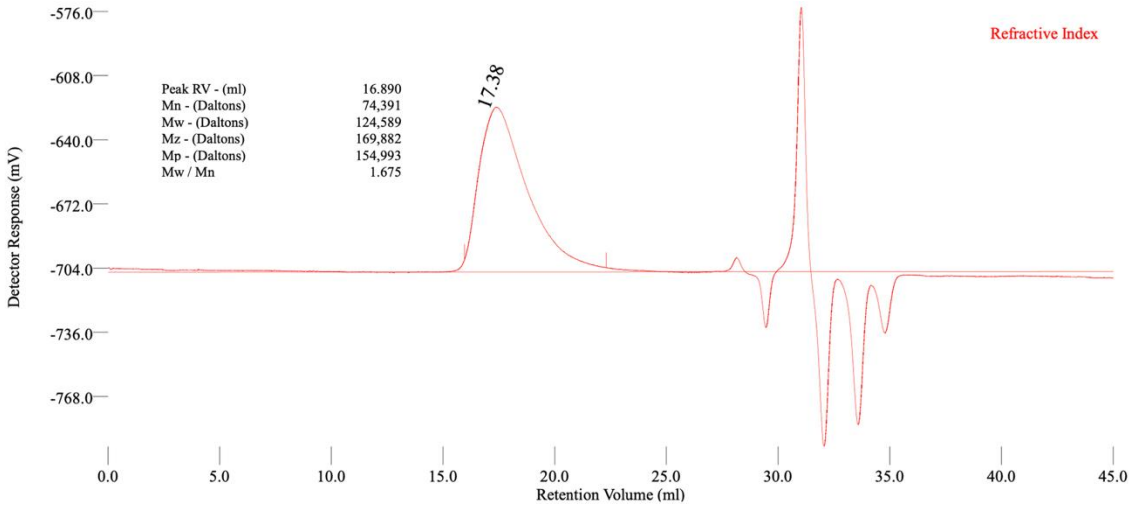

Figure S46. GPC traces of poly (*D*-LA -*co*- GA) (Table 3, entry 2).

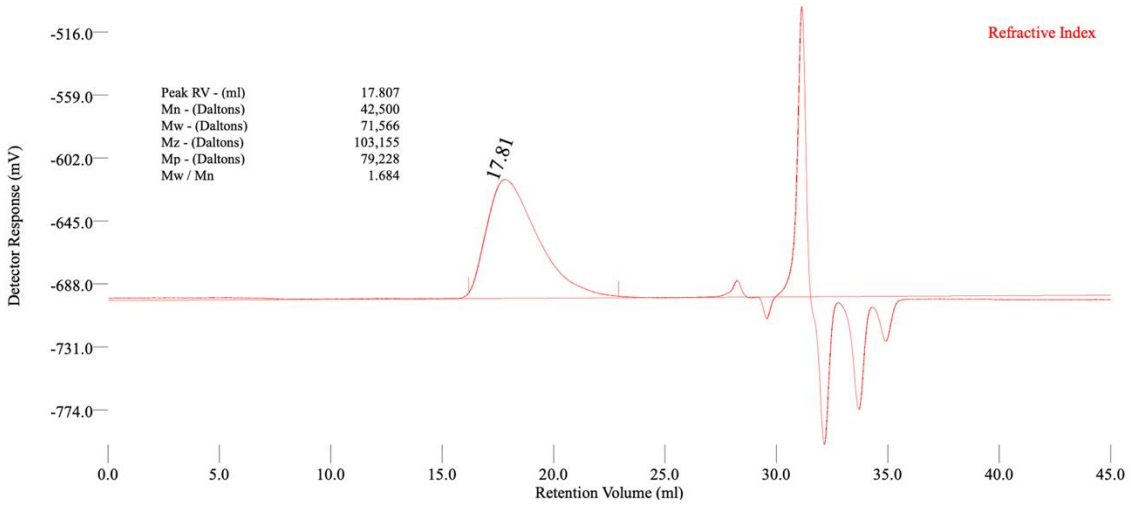

Figure S47. GPC traces of poly (*L*-LA -*co*- CL) (Table 3, entry 3).

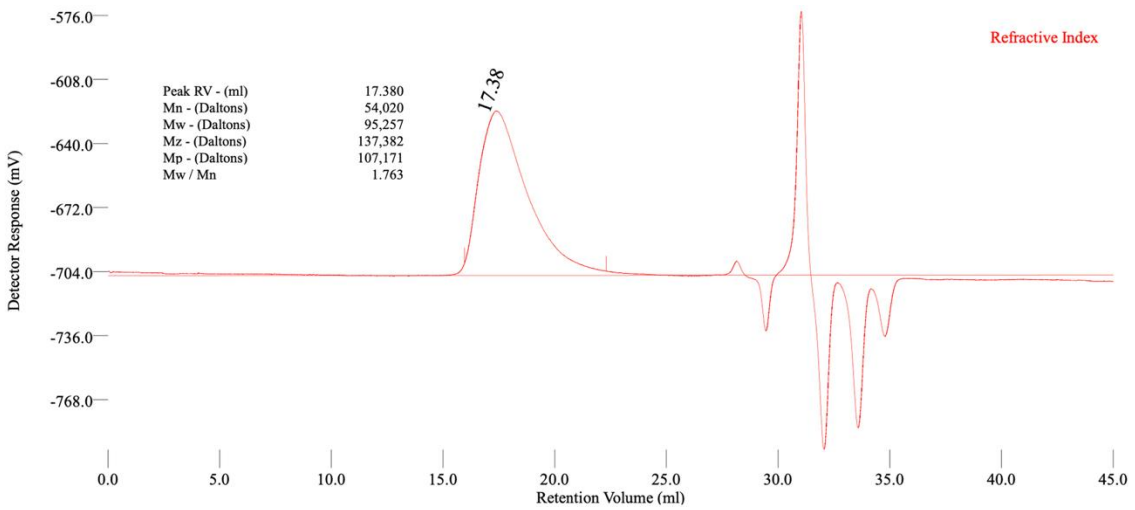

Figure S48. GPC traces of poly (*D*-LA -*co*- CL) (Table 3, entry 4).

Higher monomer feed ratios

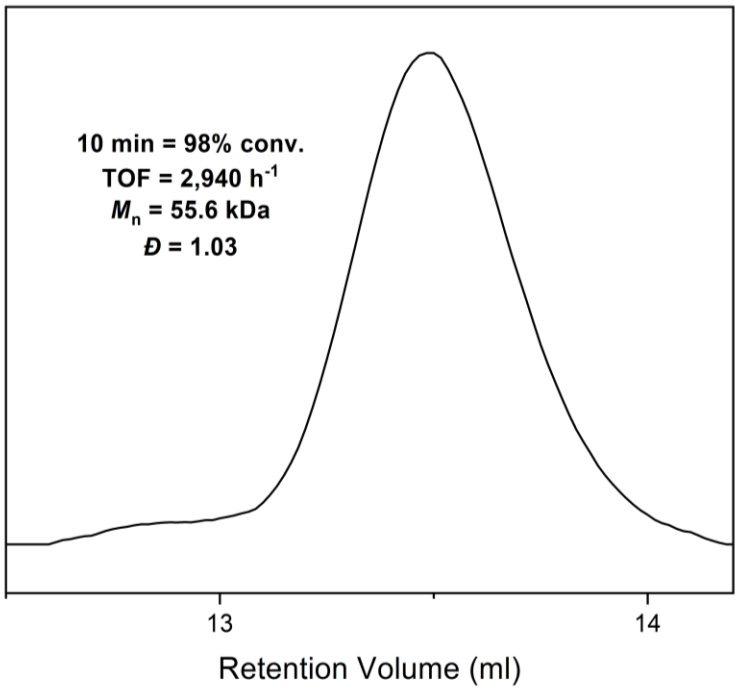

Figure S49. GPC traces of poly(*L*-LA) obtained from the polymerization of 500 equiv. of *L*-LA catalyzed by **2c** (Table 1, entry 5)**.**

Sequential addition polymerization

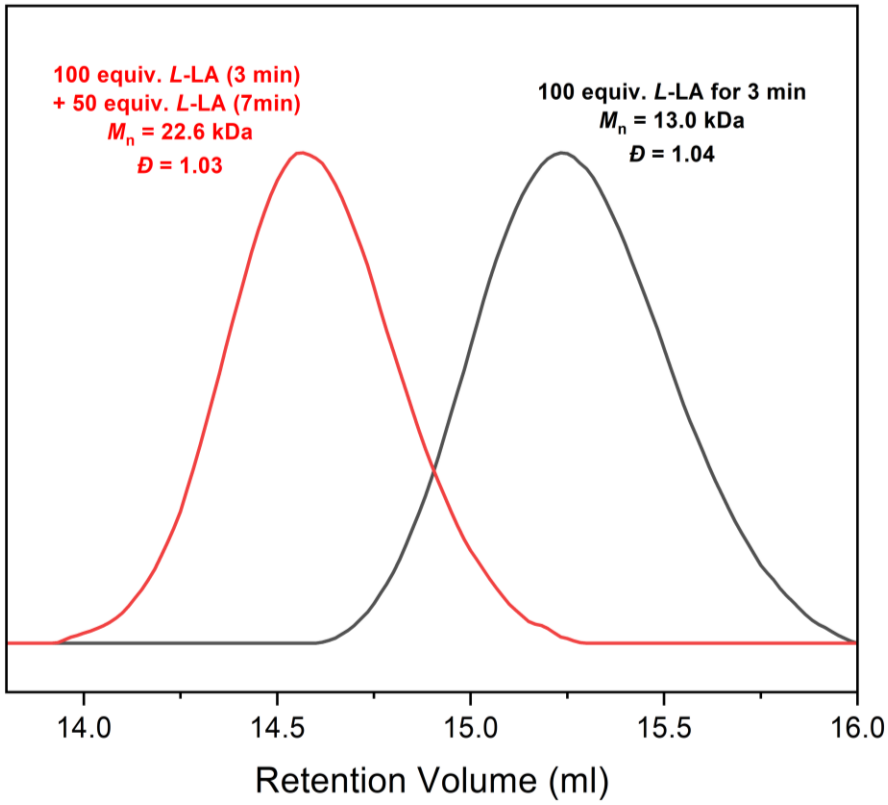

Figure S50. GPC traces of poly(*L*-LA) obtained by sequential addition of 100 equiv. of *L*-LA for 3 min (black color), waited for 15 min, and followed by an additional of 50 equiv. of *L*-LA for additional 7 min (red color).

Single-Crystal X-ray Crystallography

Table S2. Crystal data and structure refinement for complex **2a, 2b**, and **2c**

Complex	**2a**	**2b**	**2c**
CCDC	2489168	2489169	2489170
Chemical formula	$C_{40}H_{59}InN_2O_3$	$C_{41}H_{61}InN_2O_3 \cdot C_3H_7 \cdot C_3H_3$	$C_{44}H_{65}InN_2O_3$
Formula weight	730.71	826.87	784.80
Temperature (K)	100	100	100
Wavelength (Å)	1.54178	1.54178	0.71073
Space group	$P2_12_12_1$	$P2_1/c$	Cc
Crystal size (mm)	0.35 × 0.13 × 0.05	0.18 × 0.17 × 0.10	0.16 × 0.14 × 0.05
Crystal system	Orthorhombic	Monoclinic	Monoclinic
a (Å)	10.019 (3)	19.445 (8)	10.293 (7)
b (Å)	17.802 (6)	11.725 (5)	33.327 (2)
c (Å)	24.811 (7)	21.287 (9)	12.318 (9)
V (Å^3)	4425.3 (2)	4394.7 (3)	4068.8 (5)
Z	4	4	4
Density (cald.) (mg/m^3)	1.097	1.250	1.281
μ (mm^{-1})	4.51	4.60	0.62
Theta range for data collection (°)	4.3 – 70.2	5.0 – 72.4	2.8–30.5
F (000)	1544	1760	1664
Reflection collected	33547	102062	56659
Unique reflections	7932	8332	11529
Goodness-of-fit-on F^2	1.05	1.07	1.07
R1(F), wR(F^2)	0.070, 0.176	0.019, 0.051	0.024, 0.053
Largest diff. peak and hole [e Å^{-3}]	2.05 and -1.36	0.59 and -0.44	1.14 and -0.50

Table S3. Selected bond distances and angles for complex **2a**

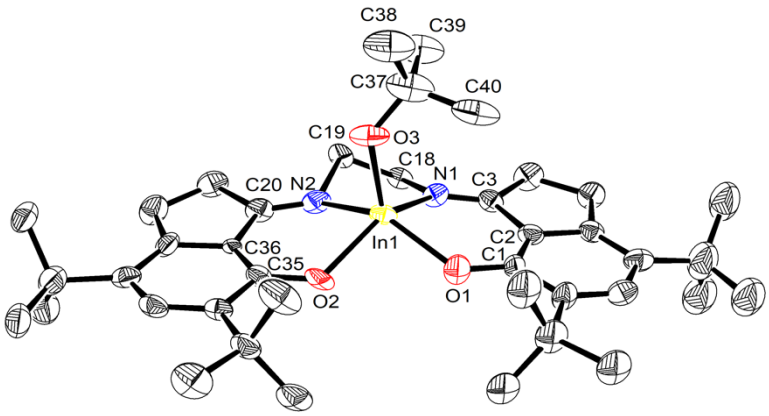

Bond distances (Å)		Bond angles (deg)	
In1—O2	2.089 (7)	O2—In1—N1	141.5 (4)
In1—O1	2.060 (8)	O2—In1—N2	85.0 (3)
In1—N1	2.207 (8)	O1—In1—O2	91.0 (3)
In1—O3	2.026 (7)	O1—In1—N1	85.7 (3)
In1—N2	2.207 (1)	O1—In1—N2	142.6 (4)
O1—C1	1.304 (1)	O3—In1—O2	104.4 (4)
O2—C35	1.304 (1)	O3—In1—O1	115.7 (4)
O3—C37	1.361 (2)	O3—In1—N1	111.5 (4)
N1—C3	1.257 (1)	O3—In1—N2	101.2 (4)
N1—C18	1.480 (2)	N2—In1—N1	75.2 (3)
N2—C20	1.287 (2)		
N2—C19	1.504 (2)		
N1—O1	2.905 (1)		
N2—O2	2.903 (1)		

Table S4. Selected bond distances and angles for complex **2b**

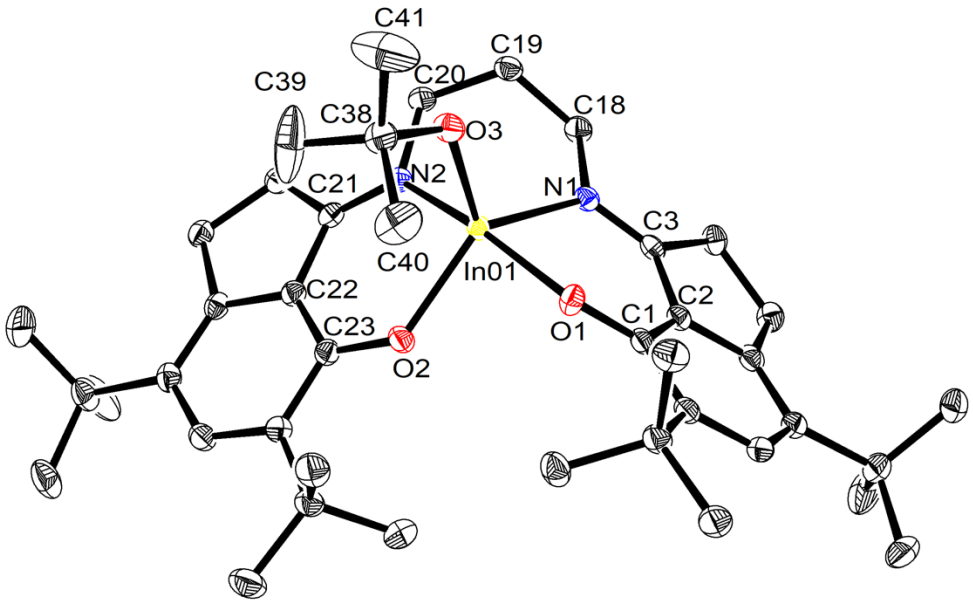

Bond distances (Å)		Bond angles (deg)	
In01—O1	2.107 (9)	O1—In01—N1	85.1 (4)
In01—O2	2.092 (9)	O1—In01—N2	162.7 (4)
In01—O3	2.025 (9)	O2—In01—O1	89.3 (4)
In01—N1	2.194 (1)	O2—In01—N1	125.4 (4)
In01—N2	2.259 (1)	O2—In01—N2	85.3 (4)
O1—C1	1.319 (2)	O3—In01—O1	100.2 (4)
O2—C23	1.323 (2)	O3—In01—O2	120.9 (4)
O3—C38	1.425 (2)	O3—In01—N1	113.5 (4)
N1—C3	1.302 (2)	O3—In01—N2	96.6 (4)
N1—C18	1.480 (2)	N1—In01—N2	84.7 (4)
N2—C20	1.478 (2)		
N2—C21	1.293 (2)		
N1—O1	2.909 (1)		
N2—O2	2.950 (1)		

Table S5. Selected bond distances and angles for complex **2c**

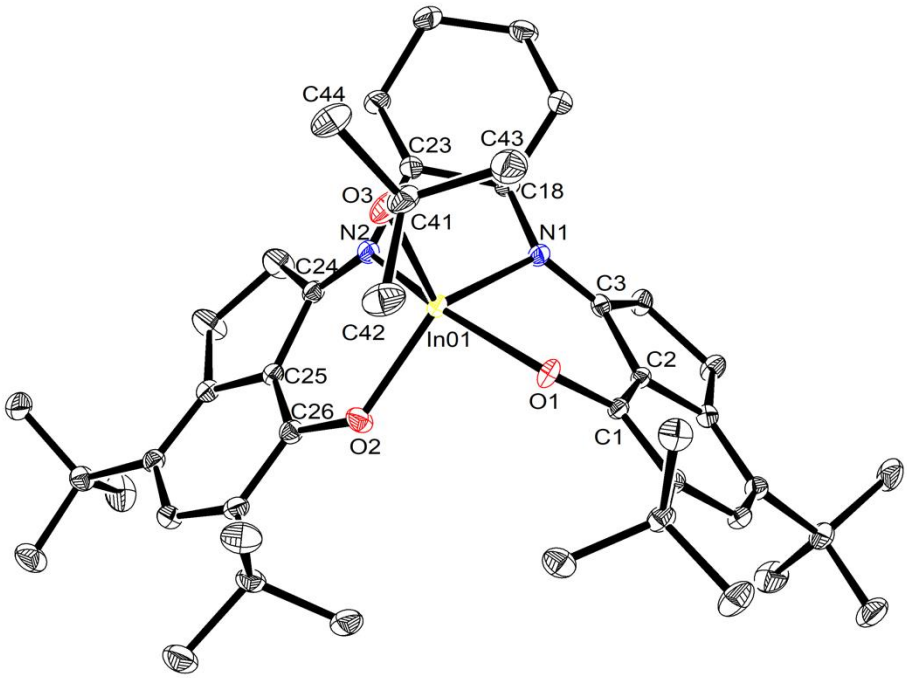

Bond distances (Å)		Bond angles (deg)	
In01—O2	2.057 (2)	O2—In01—O1	95.9 (7)
In01—O1	2.083 (2)	O2—In01—N2	86.8 (8)
In01—O3	2.001 (2)	O2—In01—N1	127.0 (8)
In01—N2	2.232 (2)	O1—In01—N2	152.9 (8)
In01—N1	2.219 (2)	O1—In01—N1	84.6 (7)
O1—C1	1.320 (3)	O3—In01—O2	116.7 (9)
O2—C26	1.324 (3)	O3—In01—O1	109.2 (8)
O3—C41	1.399 (3)	O3—In01—N2	93.3 (8)
N1—C3	1.294 (3)	O3—In01—N1	112.8 (9)
N1—C18	1.474 (3)	N1—In01—N2	72.5 (8)
N2—C23	1.472 (3)		
N2—C24	1.282 (3)		
N1—O1	2.898 (1)		
N2—O2	2.951 (1)		

References

1. B. M. Chamberlain, M. Cheng, D. R. Moore, T. M. Ovitt, E. B. Lobkovsky and G. W. Coates, *J. Am. Chem. Soc.*, 2001, **123**, 3229-3238.
2. P. Dobrzynski, J. Kasperczyk, H. Janeczek and M. Bero, *Macromolecules*, 2001, **34**, 5090-5098.
3. J. Kasperczyk, *Polym.*, 1996, **37**, 201-203.
4. H. R. Kricheldorf and I. Kreiser, *Die Makromol. Chem.*, 1987, **188**, 1861-1873.
5. J. Yoo, D. Viswanath and Y.-Y. Won, *ACS Macro Lett.*, 2021, **10**, 1510-1516.
6. P. Chumsaeng, S. Haesuwannakij, A. Virachotikul and K. Phomphrai, *J. Polym. Sci., Part A: Polym. Chem.*, 2019, **57**, 1635-1644.
7. J. Kasperczyk and M. Bero, *Die Makromol. Chem.*, 1993, **194**, 913-925.
8. L. Mezzasalma, S. Harrisson, S. Saba, P. Loyer, O. Coulembier and D. Taton, *Biomacromolecules*, 2019, **20**, 1965-1974.
9. in *Principles of Polymerization*, John Wiley & Sons, Inc., Hoboken, New Jersey., 2004, DOI: https://doi.org/10.1002/047147875X.ch6, ch. 6, pp. 464-543.